

Synthesis, spectral properties, α -glucosidase inhibition, second-order and third-order NLO parameters and DFT calculations of Cr(III) and V(IV) complexes of 3-methylpicolinic acid

Davut Avcı^{a*}, Sümeyye Altürk^a, Fatih Sönmez^b, Ömer Tamer^a, Adil Başoğlu^a, Yusuf Atalay^a, Belma Zengin Kurt^c, Necmi Dege^d

^aSakarya University, Faculty of Arts and Sciences, Department of Physics, 54187, Sakarya, Turkey

^bSakarya University of Applied Sciences, Pamukova Vocational High School, 54055, Sakarya, Turkey

^cBezmialem Vakıf University, Faculty of Pharmacy, Department of Pharmaceutical Chemistry, 34093 Istanbul, Turkey

^dOndokuz Mayıs University, Faculty of Arts and Sciences, Department of Physics, 55139, Samsun, Turkey

Abstract: The Cr(III) and V(IV) complexes of 3-methylpicolinic acid (3-mpaH) were synthesized. The XRD and LC-MS/MS were performed to determine experimental geometric structure of the synthesized complexes. Their experimental spectral analyses were carried out by FT-IR and UV-Vis spectra. Their α -glucosidase activities were also evaluated. The synthesized Cr(III) and V(IV) complexes exhibited α -glucosidase inhibitory activity with the IC₅₀ values of >600 μ M. Furthermore, the optimal molecular structure geometries, vibrational frequencies, electronic spectral properties, refractive index, band gap, second- and third-order nonlinear optical (NLO) parameters of these complexes were obtained by using DFT/HSEh1PBE/6-311G(d,p)/LanL2DZ level. NLO results demonstrate that the complex **1** is a promising candidate to materials with the high first- and second-order hyperpolarizability values obtained at 55.3×10^{-30} and 251.0×10^{-36} esu in ethanol solvent. The experimental refractive index and band gap parameters were comparatively presented. Lastly, NBO analysis was fulfilled to investigate inter- and intra-molecular bonding and the definition of coordination geometries around the central metal ions, as well as the electronic charge transfer interactions in the Cr(III) and V(IV) complexes.

Keywords: 3-Methylpicolinic acid; spectral analysis; α -glucosidase; refractive index and NLO; DFT/HSEh1PBE.

* Corresponding author. E-mail: davci@sakarya.edu.tr (D. Avcı).
Tel: +90 264 295 6097; fax: +90 264 295 5950.

1. Introduction

The metal complexes of nitrogen-containing heterocyclic ligands have been commonly received great attention in the different fields due to their potential applications until today [1-6]. In addition, by virtue of the structural, spectroscopic and catalytic similarities to important enzyme-substrate complexes in the human body, as well as their applications in non-linear optics, coordination and bio-material chemistry, various metal complexes of pyridine derivatives have been reported [7-11]. The determine roles of metal complexes in biological processes such as diabetes mellitus (DM) which is characterized by a high level of blood glucose, are crucial. Furthermore, type 2 diabetes (T2DM) is expected to be one of the ten fatal diseases in the coming years according to the report of the world health organization (WHO). In this respect, the searches for efficient antidiabetic treatments are important to reduce blood glucose levels and keep glucose under control. It has been declared that α -glucosidase inhibitors improve postprandial hyperglycemia and subsequently decrease the risk of developing type 2 diabetes [12-14]. The design and synthesis of the glucosidase inhibitors with high efficiency were taken account as one of the intensive research fields due to the therapeutic effects of the complexes with different metal ions on individuals suffering from type 2 diabetes [15-20]. Although the synthesis, some spectral properties and computational studies of copper(II), nickel(II), cobalt(II), lead(II), vanadium(IV) complexes with 3-methylpicolinic acid have been reported [21-26], there are no α -glucosidase enzyme activity studies of the Cr(III) and V(IV) complexes of 3-mpaH ligand in the literature. The synthesis, characterization, electrochemical properties and biological activity study for ruthenium(II) complex of 2,2'-bipyridine with 3-methylpicolinic acid were also fulfilled [27].

It is clear from the literature that no detailed studies have been conducted on the NLO properties of these materials. But in recent years, the studies of NLO features with different application areas such as optical communication, information storage and optical switching have been attracted attention in optoelectronic technology. Thanks to this situation, a number of experimental and theoretical studies are carried out [28-34]. The optical nonlinearity of organic, inorganic and organometallic compounds can be amplified either by conjugated bonds or by binding of electron donor and acceptor groups.

Some compounds especially non-centrosymmetric organic compounds including the electron-donor (D)- π -electron acceptor (A) or A- π -D type structures have been extensively investigated due to the possibility of having a great value of first hyperpolarizability (β) [35-41]. But, the achieve of NLO properties for the complex structures containing transition metals is a key importance because of non-centrosymmetric or centrosymmetric coordination geometries around the central metal ions. It is clear that the differences in the obtained NLO parameters (first- and second-hyperpolarizability (β and γ)) could be observed in the literature for structures with this type of coordination geometry [17-20,28-31]

It could be considered that the high difference of dipole moment between the ground and excited state for the organic molecules is obtained due to the strong intramolecular charge transfer (ICT) originated from donor to acceptor units through π -bridge [35-41]. However, the NLO response of the donor and acceptor units around the metal ions acting as π -bridge in the transition metal complexes could be provided to observe the dominant electronic transitions. Hence, the two-state model [35-48] has been commonly used to determine NLO response in the donor-acceptor compounds. Moreover, these push-pull configurations lead to not only reduce the HOMO-LUMO energy gap and increase the NLO response, but also help to increase asymmetrical electronic distribution and extend the absorption range to a longer wavelength. Considering the results previously reported for first hyperpolarizabilities obtained by using the different theoretical approaches (HSEh1PBE, B3LYP, M062X, CAM-B3LYP and BHandHLYP), the HSEh1PBE/6-311G(d,p) level was found as consistent with

the experimental results [47]. In a previous study, the NLO parameters were calculated at the hybrid GGA, meta-GGA, range-separated hybrid and LR corrected DFT models (B3LYP, B3PW91, M062X, HSEh1PBE, CAM-B3LYP, LC-BLYP and xB97XD) in the gas phase and methanol [49], and it is reported that the hybrid meta-GGA B3LYP, B3PW91 methods and range separated hybrid HSEh1PBE level were found to be more comparable results than the other M062X, CAM-B3LYP, LC-BLYP and xB97XD methods incorporating the high amount LR-HF% exchange. These results are important for the determination of the calculation method in different molecular structures. In this context, according to the previously obtained results for the different metal complex [17-20,28-31] and organic compounds [50-52], the HSEh1PBE method was chosen for the investigating of the spectral and NLO properties.

The main purpose of the present study is to synthesize Cr(III) and V(IV) complexes of 3-methylpicolinic acid (3-mpaH) and come out the detailed structure-activity relations of these complexes. The investigation of the α -glucosidase enzyme activity, linear and nonlinear optical parameters for Cr(III) and V(IV) complexes have not been fulfilled though the V(IV) complex of 3-mpaH was previously synthesized and its spectroscopic (EPR, UV-vis, and IR spectroscopy) and computational calculations were performed [26]. Synthesis, structural, chemical and bioactivity behavior for Cr(III) complex of 3-mpaH were carried out [53]. The crystal structure of complex **1** [Cr(3-mpa)₃] was defined by XRD spectroscopic technique and molecular structure of complex **2** [VO(3-mpa)₂] was determined by mass spectrometry (MS). The α -glucosidase enzyme inhibition, vibrational and electronic absorption spectra, refractive index, as well as optical band gap parameters were experimentally examined. To reveal structure-activity relations, the detailed theoretical calculations by using DFT/HSEh1PBE/6-311G(d,p)/LanL2DZ level in the gas phase and ethanol solvent were carried out for the structural, vibrational, electronic, linear- and non-linear optical parameters of complexes **1** and **2**. Finally, the ligand protein interactions were determined by molecular docking.

2. Experimental and Computational Procedures

2.1. General remarks

All chemicals used in the synthesis process of Cr(III) and V(IV) complexes are analytical grade commercial products. 3-mpaH (3-methylpicolinic acid), chromium(III) nitrate nonahydrate (Cr(NO₃)₃·9H₂O) and vanadium(IV) oxide sulfate hydrate (VOSO₄·xH₂O) were purchased from Sigma-Aldrich.

The single crystal X-Ray diffraction (XRD) [54-56] and LC-MS/MS methods as well as FT-IR and UV-Vis spectrophotometer used to analyze geometric and spectroscopic properties of Cr(III) and V(IV) complexes were presented in the Supplementary Material.

2.2. Synthesis of the complexes **1** and **2** {[Cr(3-mpa)₃], (**1**), [VO(3-mpa)₂], (**2**)}.

Synthesis procedures of the complexes **1** and **2** are as follows (Scheme 1):

To a solution of the 3-methylpicolinic acid and trimethylamine (3 mmol) dissolved in water (15 mL) was dropped the solution of chromium(III) nitrate nonahydrate (1 mmol) dissolved in water (5 mL). This mixture was stirred at 100 °C for 1h and then evaporated for 15 days at room temperature. At the end of this process, the occurred suitable single crystals with prism-shaped for complex **1** were collected. Yield: 74.6%.

The 3-methylpicolinic acid (2 mmol) and vanadium(IV) oxide sulfate hydrate (1 mmol) were dissolved in water (10 mL). Then an aqua solution (1.5 mL) of sodium bicarbonate (0.12 M) was added to the mixture. It was stirred at room temperature for 3 h and evaporated for 15 days at room temperature. At the end of this process, the powder product

for complex **2** was obtained. Yield: 43.5%. Anal. Calc. for $C_{14}H_{12}N_2O_5V$ (complex **2**): C, 49.57; H, 3.57; N, 8.26. Exact mass (m/z): 362.02. Found: C, 49.43; H, 3.85; N, 8.23. ESI-LC-MS/MS (m/z): 365.1 ($[M]^+$). Fig. S1 displays the mass spectrum of the complex **2**.

2.3. α -Glucosidase inhibition assay

The α -glucosidase activities of the synthesized complexes **1** and **2** were determined on the basis of our previous studies [17-20]. The detailed inhibition method was presented in Supplementary Material. The determination inhibition activities for the complexes **1** and **2** against α -glucosidase was carried out by the following equation,

$$\text{Glucosidase inhibition} = [(A_c - A_s)/A_c] \times 100 \quad (1)$$

where A_c and A_s are the absorbance of control and samples, respectively. Graphpad Software was also utilized to calculate IC_{50} .

2.4. Computational details

The density functional theory calculations on the complexes **1** and **2** were fulfilled by using GAUSSIAN 09, Revision D01, [57] and GaussView 5 program [58].

The unrestricted DFT calculations were carried out for the complexes **1** and **2** containing Cr and V ions, respectively. The stable spin states for the complexes **1** and **2** including Cr and V ions are doublet. Although the EDIIS + DIIS method for SCF convergence was used, no particular problems were encountered. This method contains the following calculation criterion: the Harris functional diagonalization for initial guess, and convergence which stops the SCF when the RMS deviation between elements of successive density matrices is smaller than 10^{-8} and the change in energy is below 10^{-6} . It is stated that the $\langle S^2 \rangle$ values for all DFT calculations were considered in the range 0.7500–0.7960, these values in the gas phase and ethanol solvent are calculated at the value of 0.7696 and 0.7714 (for complex **1**), 0.7618 and 0.7616 (for complex **2**) in the ground state calculations, as expected. These results are accepted to be suitable for spin doublet states in the ground state calculations. So, the obtained lowest energy structures for the complexes **1** and **2** in this spin state were used the investigation of the molecular properties.

The optimized molecular structures and vibrational wavenumbers for the complexes **1** and **2** were evaluated by using DFT/HSEh1PBE [59,60] method in conjunction with the combined basis set of 6-311G(d,p) [61] for C, N, O, H atoms and LanL2DZ [62] for Cr and V atoms. The same methods in the gas phase and ethanol solvent were applied to examine the microscopic linear polarizability ($\bar{\alpha}$ and $\Delta\alpha$), first- and second-hyperpolarizability (β and γ), refractive index (n) parameters. The $\bar{\alpha}$, $\Delta\alpha$, β and γ parameters were obtained by using following equations [42-47]:

$$\langle a \rangle = \frac{(a_{xx} + a_{yy} + a_{zz})}{3} \quad (2)$$

$$\Delta\alpha = \left\{ \frac{1}{2} \left[(a_{xx} - a_{yy})^2 + (a_{yy} - a_{zz})^2 + (a_{zz} - a_{xx})^2 \right] \right\}^{1/2} \quad (3)$$

$$\beta = (\beta_x^2 + \beta_y^2 + \beta_z^2)^{1/2} \quad (4)$$

$$\langle \gamma \rangle = \frac{1}{5} [\gamma_{xxxx} + \gamma_{yyyy} + \gamma_{zzzz} + 2(\gamma_{xxyy} + \gamma_{xxzz} + \gamma_{yyzz})] \quad (5)$$

where the cartesian components of $\bar{\alpha}$, $\Delta\alpha$ and β are a_{xx} , a_{yy} , a_{zz} , $\beta_x = \beta_{xxx} + \beta_{xyy} + \beta_{xzz}$, $\beta_y = \beta_{yyy} + \beta_{yxx} + \beta_{yzz}$, $\beta_z = \beta_{zzz} + \beta_{zyy} + \beta_{zxx}$. The atomic units of $\bar{\alpha}$ and β are converted to esu. 1 atomic unit (a.u.) = 0.1482×10^{-24} electrostatic unit (esu) for $\bar{\alpha}$ and 1 a.u. = 8.6393×10^{-33} esu for β .

In order to determine the coordination geometries around the central metal ions and demonstrate the hydrogen bonding interaction, natural bond orbital (NBO) study [63] was performed.

The stability energy $E^{(2)}$ for each donor (i) and acceptor (j) was calculated by the following equation [29,31,64,65],

$$E^{(2)} = \Delta E_{ij} = q_i \frac{F(i,j)^2}{\varepsilon_i - \varepsilon_j} \quad (6)$$

where ε_i and ε_j are diagonal elements, $F(i,j)^2$ is the off-diagonal NBO Fock matrix elements, and q_i is the donor orbital occupancy.

So as to survey the electronic absorption wavelengths, oscillator strengths, major electronic transitions of the complexes **1** and **2** in ethanol solvent and gas phase, the time dependent DFT (TD-DFT) level [66] with the conductor-like polarizable continuum model (CPCM) [67] was used. After all, the molecular parameters (η : Chemical hardness, χ : Electronegativity and S : Chemical softness) obtained from frontier molecular orbital (FMO) energies were computed by using HSEh1PBE level. The η , χ and S parameters were computed by following equations [28,29,68].

$$\eta = \frac{(E_{LUMO} - E_{HOMO})}{2} \quad (7)$$

$$\chi = -\frac{(E_{HOMO} + E_{LUMO})}{2} \quad (8)$$

$$S = \frac{1}{\eta} \quad (9)$$

3. Results and discussion

3.1. The structural analysis of the complexes **1** and **2**

The synthesis routes for the complexes **1** and **2** were given in Scheme 1. The molecular structures of the complexes **1** and **2** were defined by X-ray diffraction technique and mass spectrometry (MS), respectively. Fig.1 demonstrates the single crystal molecular structure and ground state optimized molecular structures of the title complexes. Crystal data and structure refinement parameters for the complex **1** were tabulated in Table 1. The crystal structure of complex **1** is similar to crystal structure of Cr(3-mpa)₃ complex reported previously [53], and it crystallizes in monoclinic C2/c space group (Table 1).

It is clear from Fig. 1 that the coordination geometry around Cr(III) atom for the complex **1** was determined as distorted octahedral geometry while the coordination around V(IV) metal for complex **2** was described as a distorted square-bipyramidal. The complex **1** consists of Cr(III) central ion coordinated by three 3-mpa ligands whereas the complex **2** comprises of the central V(IV) ion coordinated by two 3-mpa ligands and an oxygen atom.

In complex **1**, Cr–O and Cr–N bond lengths were obtained at the range from 1.930(17) to 1.949(19) Å and the range from 2.045(2) to 2.060(2) Å, respectively (Table S1). In comparison with the previous study [53], the same variation was observed in the present work. Bond angles of N2–Cr1–N3, O2–Cr1–O3, O5–Cr1–N1 were found to be 169.8(9), 172.3(8), 171.5(9)°, respectively, and these angles are coherent with the crystal structure of Cr(3mpa)₃ reported previously [53] (Table S1).

The Cr–O2/O3/O5 and Cr–N1/N2/N3 bond lengths defining five-membered chelate rings formed by coordinating to the centers of metal ions were observed at the range from 1.935(2) to 2.060(2) Å. Likewise, the V–O2/O3 and V–N1/N2 bond distances for the complex **2** were obtained at the range of 1.932–2.090 Å by using HSEh1PBE level (Table S1). These obtained results for the title complexes are consistent with previously reported picolate complexes [17-26]. When it comes to O–Cr–N and O–V–N bond angles describing five-membered chelate ring, these angles for the complexes **1** and **2** were found to be 77.0–82.1° range. Compared with corresponding parameters obtained before [17-26,53], it could be stated that a good agreement between the bond lengths and angles around the coordination environment of metal ions for the complexes **1** and **2** despite metal ion and coordination differences.

The natural bond orbital (NBO) results for the complexes **1** and **2** obtained at the HSEh1PBE/6-311G(d,p)/LanL2DZ level display that the interactions between bonds, the coordination environment of Cr(III) and V(IV) ions, as well as the conjugative interaction among ligands in the complex structures. The second-order perturbation approach is applied to obtain the hyperconjugative interaction energies [64,65]. Due to the delocalization effect observed between lone-pair (n) orbitals of nitrogen/oxygen atom and anti-lone-pair (n*) orbitals of Cr(III) and V(IV) ions, the coordination environments for the complexes **1** and **2** were confirmed by n→n* interactions. These interactions were determined with the E⁽²⁾ values described as the stabilization energy. Table S2 presents the calculated E⁽²⁾ values for the complexes **1** and **2** obtained at the range from 56.53 to 1.17 kcal/mol. On the other hand, the highest stabilization energy (E⁽²⁾) values of the LP(2)O1/O4/O6→σ*(O2–C1)/(O3–C8)/(O5–C15) interactions for the complex **1** depending the COO[−] group were obtained at 13.31, 13.90 and 12.73 kcal/mol, as can be seen in Table S2. Likewise, the interaction energy values of LP(2)O1/O4→σ*(O2–C1)/(O3–C8) for the complex **2** were found to be 13.02 kcal/mol. In the Cr(III) and V(IV) complexes, the energy values for intramolecular remarkable interactions of π(C17–C18)→π*(N3–C16) and π(C9–N2)→π*(C8–O4) were obtained at 15.87 and 4.60 kcal/mol, respectively (see Table S2). To sum up, it could be stated that the stabilization of the molecular system through the bonding and anti-bonding orbitals, interactions among bonds, and coordination around metal ions.

According to the crystal packing structure of complex **1**, the C–H⋯O type intermolecular hydrogen bonding interactions revealed between the –CH group of 3-mpa ligand and O atom of carboxylate group (see Table 2 and Fig. S2). Additionally, the other remarkable stabilization interactions in the ligands of the complex structures are given in Table S2.

3.2. Infrared spectra

Table 3 displays the experimental and theoretical vibrational wavenumbers obtained by hybrid HSEh1PBE method and 6-311G(d,p)/LanL2DZ basis set, and then scaled by 0.96. The FT-IR spectra and theoretical calculations are used to determine the coordination environment around the metal ions and the other assignments of vibrational modes for the complexes **1** and **2**. The FT-IR spectra are given as two parts, the first one is at the range of 4000–400 cm^{−1}, and second one is in the region of 1750–400 cm^{−1} (see Fig. 3a and 3b). These

spectra and theoretical results verify the coordination of 3-mpa ligand to Cr(III) ion and 3-mpa ligand to V(IV) ion via the carboxylate group in the complexes **1** and **2**, respectively. The asymmetric/symmetric stretching COO^- ($\nu_{\text{as}}/\nu_{\text{s}} \text{COO}^-$) vibrational modes from FT-IR spectra of complexes **1** and **2** were observed at 1665/1270 and 1627/1250 cm^{-1} , respectively. The corresponding theoretical vibrational bands were found to be 1741/1267 and 1627/1260 cm^{-1} . The differences between the experimental/theoretical ν_{as} and ν_{s} COO^- vibrational modes obtained at 395/474 for complex **1** and 377/481 cm^{-1} for complex **2** demonstrate the presence of carboxylate group coordinated to Cr(III) and V(IV) ions, respectively. These results are in agreement with previously reported results [17,21-27]. Furthermore, possible differences between compared results are originated from the presence of Cr(III) and V(IV) ions including the *N,O*-chelating 3-mpa ligands for the complexes **1** and **2**.

In complex **2**, the ν VO vibrational mode, indicating comprise of the central V(IV) ion coordinated by an oxygen atom, is experimentally and theoretically obtained at 1079 and 1093 cm^{-1} (see Table 3). These results are coherent with previously observed at 966 cm^{-1} with experimental IR, and calculated at 1102, 1079, 1106 cm^{-1} with the B3P86/6-311G, B3LYP/6-311G, and PBE/6-311G levels [26]. The stretching absorptions (ν C=N and ν C=C) belong to 3-mpa ligand for the complex **1** were experimentally and theoretically assigned as 1640 and 1588 cm^{-1} , respectively. On the other hand, the CN and CC single bond stretches were observed at 1189 and 1045 cm^{-1} for the complex **1** and 1280 and 1047 cm^{-1} for the complex **2**. The corresponding theoretical vibrational modes are 1199 and 1061 cm^{-1} for the complex **1** and 1315 and 1062 cm^{-1} for the complex **2**, respectively. Observed lower vibrational modes exhibit the presence of pyridine rings coordinated to Cr(III) and V(IV) ions. These results are in agreement with the previous corresponding ones [17,21-24]. The other detailed assignments of vibrational modes for the complexes **1** and **2** are assigned in Table S3.

3.3. The UV-vis spectra, molecular parameters and molecular electrostatic potential surfaces

The experimental absorption spectra of the complexes **1** and **2** in ethanol solvent were recorded at the range from 900 to 200 nm, and presented in Fig. 3. TD-HSEh1PBE method with 6-311G(d,p)/LanL2DZ basis sets were used to calculate electronic absorption wavelengths and transitions, and oscillator strengths. The important contributions from FMOs were obtained by using SWizard and Chemissian software [69,70]. Obtained these parameters were collected in Table 4. At the same time, the HSEh1PBE level was also chosen to provide a tendency to interpret between current complex results and the previously obtained results in the different metal complexes [17-20,28,29,31].

There are four wide absorption bands ($\lambda_{\text{max}} = 321, 270, 260$ and 218 nm) observed in the UV-Vis absorption spectrum of the complex **1**. Similarly, three wide absorption bands for the complex **2** appeared at 371, 273 and 210 nm in the ethanol solvent (see Fig. 3). But these bands were measured at 740, 560 and 385 nm in the aqueous solution [26]. On the whole, the data are comparable in spite of the solvent difference. At the same time, the experimental UV-Vis spectrum of the 3-mpaH displays that two absorption bands emerged at 270 and 216 nm in the ethanol solvent (see Fig. 3). Theoretical corresponding absorption peaks of the complexes **1** and **2** in ethanol solvent were found to be 523-246 and 587-224 nm range, respectively. Besides, the differences between TD-DFT results and recorded UV-Vis spectra are dependent on the selected number of excited states in TD-DFT calculations. In this study, the electronic absorption parameters were calculated by using the different theoretical approaches (B3LYP and CAM-B3LYP levels). The results of B3LYP and CAM-B3LYP levels corresponding absorption peaks in ethanol solvent were found to be 526-256 and 528-216 nm range for complex **1**, 605-229 and 553-230 nm range for complex **2**, respectively. No significant difference was observed among the results of B3LYP, CAM-B3LYP and

HSEh1PBE levels. Furthermore, the detailed contributions from COO⁻ (carboxylate) group, 3-mepy (3-methylpyridine) ligand, Cr and V metal ions to absorption peaks of the complexes **1** and **2** in ethanol solvent are given in Table 4. The theoretical peak of 587 nm of the complex **2** with the molecular orbital contributions of H→L+4 α(44%) and H→L+1α(25%) were appointed as a metal-ligand charge transfer (MLCT) transition depending on VO(59%)+3-Mepy(23%)+COO⁻(18%)→VO(50%)+3-Mepy(48%)+COO⁻(2%) and VO(59%)+3-Mepy(23%)+COO⁻(18%)→VO(10%)+3-Mepy(80%)+COO⁻(10%), as can be seen in Table 4. The remarkable absorption peaks of the complexes **1** and **2** in ethanol solvent emerged at 321 and 371 nm were attributed to between metal–ligand and ligand–ligand charge transfer. Theoretical corresponding ones were obtained at 395 and 400 nm. These transitions determined by the electronic contributions of H→L+3α(+48%)/Cr(61%)+3-Mepy(27%)+COO⁻(12%)→Cr(11%)+3-Mepy(77%)+COO⁻(12%) for the complex **1** and H→Lα(+77%)/VO(59%)+3-Mepy(23%)+COO⁻(18%)→VO(7%)+3-Mepy(80%)+COO⁻(13%) for the complex **2**. The other absorption peaks of the complexes **1** and **2** in ethanol solvent observed at 270 and 218, 273 and 210 nm were assigned as n→π* and π→π* transitions, indicating ligand–ligand charge transfer. For example, the absorption peak at 210 nm of the complex **2** was determined by the electronic contributions of H–8→L+1α(+38%)/3-Mepy(25%)+COO⁻(65%)→3-Mepy(80%)+COO⁻(10%) and H–6→L+1β(+20%)/3-Mepy(26%)+COO⁻(65%)→3-Mepy(83%)+COO⁻(11%). It is concluded from Fig. 4 and Table 4 the low absorption values of the complexes **1** and **2** are based on possible intra-ligand charge transfer (ILCT).

Considering the two-state model [35-48], it is intended to set up the relation of hyperpolarizability and charge transfer transition in the foresight proficient NLO systems.

$$\beta_0 \propto \frac{\Delta\mu_{eg} f}{E_{eg}^3} \quad (10)$$

In eq. (10), $\beta_0, \Delta\mu_{eg}, E_{eg}, f$ are the first static hyperpolarizability also denoted as β_{CT} , dipole moment difference between ground and excited states, transition energy, and oscillator strength associated with the electronic transition from the ground state to the predominant charge transfer excited states, respectively.

According to the two-level model [42,45], eq. 1 can be denoted as eq. 2. The static first hyperpolarizability (β_0) is given by the simple formula [43,44,46,47].

$$\beta_0 = (3.79597 \times 10^{-7}) \mu_{eg}^2 \Delta\mu \lambda_{eg}^2 \quad (11)$$

In eq. (11), μ_{eg} (in D) is the transition dipole moment between the ground and excited states, $\Delta\mu = \mu_e - \mu_g$ (in D) is the difference in dipole moment between the ground and first excited states, λ_{eg} (in nm) is the excitation wavelength. When above units are used, β_0 is obtained in 10^{-30} esu together with the 3.79597×10^{-7} constant. It is clear from the two-level model that first hyperpolarizability increases with the large $\mu_{eg}, \Delta\mu$ values and λ_{eg} , or the lower transition energy. Depending on the π -conjugation length linking the electron–acceptor and –donor groups in the push–pull type systems, it should be stated that the higher β_0 hyperpolarizability is the lower transition energy, and the higher oscillator strength and the difference between ground and excited state dipole moment [47,48]. The calculated values of μ_{eg}, f and λ_{eg} were presented in Table 4 and the obtained $\Delta\mu$ and β_0 results were given in Table 5. It is clear from Table 4 the highest values of λ_{eg} for the complexes **1** and **2** in ethanol/gas phase

corresponding to maximum oscillator strength were calculated at 395/414 nm and 252/247 nm, respectively. The μ_{eg} and $\Delta\mu$ values for the complex **1** in ethanol/gas phase were found to be 1.8394/2.1984 D and 1.7/0.6 D (see Tables 4 and 5). To contribute to the second-order NLO property of the complexes **1** and **2**, the relationship between $\langle\beta\rangle$ (the mean first-order hyperpolarizability) values and β_0 (two-level model) values were investigated and calculated. These results were tabulated in Table 5. At the same time, the two-level model was associated with the UV-vis properties. The β_0 (two-level model) values for the complexes **1** and **2** in ethanol/gas phase were obtained at 0.341/0.189 ($\times 10^{-30}$) esu and -0.166/-0.0255 ($\times 10^{-30}$) esu, respectively. It could be stated that these results display the same tendency as the $\langle\beta\rangle$ parameter with regard to increase and decrease. Depending on the coordination environment and symmetry center around metal ions, the first hyperpolarizability parameters of these complexes were obtained at low values indicating little NLO response.

Based on the Tauc and Menth's equation [28,71], the direct band gap energy values for the complexes **1** and **2** are computed by using the following equation

$$(\alpha h\nu) = C(h\nu - E_g)^{1/2} \quad (12)$$

In eq. (12), α called as the absorption coefficient is obtained by $\alpha = -2.303 \log T / d$ (T is the transmittance and d called the length of the cuvette is used in 1 cm), C is a constant for the effective masses associated with the bands, h is Planck constant, ν is frequency of light and E_g is the direct band gap energy.

It is noted that the energy gap (band gap energy) between HOMO and LUMO energy indicates the chemical reactivity, molecular hardness and softness, as well as biological activity of the molecular systems. On the other hand, the smaller energy gap defines a chemically soft molecule, indicating easily polarizable and more advanced biological activity. It is clear from Fig. 5 that the E_g band gaps for the complexes **1** and **2** are 4.35 and 4.30 eV, respectively. The corresponding energy gaps calculated from FMO energies are 2.60 for α spin, 2.40 for β spin (for complex **1**), 3.90 for α spin, 4.88 eV for β spin (for complex **2**). These results are comparable with the obtained experimental results and previously reported result about 4 eV for complex **2** [26]. The χ (electronegativity), η (chemical hardness) and S (chemical softness) parameters computed from FMO energies are examined by using the previous equations [28,29,68]. The χ , η and S of the complexes **1** and **2** were obtained at 4.55 eV, 1.30 eV, 0.77 eV⁻¹ for α spin and 4.51 eV, 1.95 eV, 0.51 eV⁻¹ for β spin, respectively. These results demonstrate that the complex **1** would provide the efficient charge transfer, which has easily polarized.

The molecular electrostatic potential (MEP) surfaces of the complexes **1** and **2** were investigated to examine the relationship among the structure, physicochemical and reactivity properties [72,73]. MEP surfaces were also utilized to simultaneously determine molecular structure, size and ESP regions specified by color classification. The MEP surfaces for the complexes **1** and **2** were drawn in Fig. 6. These values for the complexes **1** and **2** are range from -7.788e-2 to 7.788e-2 a.u. and -6.687e-2 to 6.68771e-2 a.u., respectively. The electrophilic reactivity, demonstrating the negative regions with red color, are over the electronegative O atoms belonging the carboxylate group uncoordinated with metal ions. The nucleophilic reactivity, showing the positive regions with blue color, surrounds the C-H bonds.

3.4. The refractive index, linear optical polarizability, second- and third-order nonlinear optical parameters

In optoelectronic technology, materials with NLO features are taken into account for different application areas such as optical communication and switching, information storage. In this regard, novel materials are to present providing the efficiency of electronic communication between electron accepting and donating groups, as well as displaying the structure-activity relationship [74-78].

The $\chi^{(1)}$ (linear optical susceptibility) demonstrating the linear response (i.e. linear absorption and the refractive index) and $\chi^{(3)}$ (third-nonlinear optical susceptibility) parameters defined with Z-scan technique [79-83] are important due to building the basis of experimental work including metal complexes of 3-mpa ligand with regardless of experimental measurement. The nonlinear optical effect is related to $\chi^{(n)}$ parameter. The larger $\chi^{(n)}$ means the lower applied electric field strength and the shorter path length. Besides, the large $\chi^{(n)}$ of compounds including π -electron displays the delocalization of π -electrons in compounds due to applied electric fields.

The refractive index (n) for the complexes **1** and **2** were investigated by using the following equations [28,29]

$$R = \frac{(n-1)^2 + k^2}{(n+1)^2 + k^2} \quad (13)$$

$$n = \frac{1+R}{1-R} + \sqrt{\frac{4R}{(1-R)^2} - k^2} \quad (14)$$

In eq. (14), R is called as the reflectance in the IR region, n is called as the refractive index, k is called as the extinction coefficient ($(k = \alpha\lambda/4\pi)$, α is the absorption coefficient obtained by $\alpha = -2.303 \log T / d$ (T is the transmittance and d called the powder thickness is used in 0.01 cm). Fig. 7 shows the refractive index versus the wavenumber in the IR region. The average refractive index in the mid-infrared region (4000–400 cm^{-1}) for the complexes **1** and **2** were obtained at 1.39 and 1.26.

By considering the theoretical linear optical polarizability ($\bar{\alpha}$) values in the gas phase and ethanol solvent calculated by using eq. 2, theoretical refractive index (n) values were found by using the Lorentz-Lorenz eq. (15) [29,84].

$$(n^2 - 1)/(n^2 + 2) = D\bar{\alpha}/V \quad (15)$$

In eq. (6), n is called as the refractive index, V is called as the molar volume (cm^3) and D is a multiplier depending on Avogadro's number (N_A). When $\bar{\alpha}$, V and D are used in $\times 10^{-24} \text{ cm}^3$, cm^3 and $2.523564179 \times 10^{24}$, n is directly obtained in dimensionless from eq. 4.

By considering the Lorentz approximation for the local field, the linear susceptibility ($\chi^{(1)}$) of the compounds was calculated by using below eq. (16) [29,84].

$$\chi^{(1)} = Nf\bar{\alpha} \quad (16)$$

In eq. (16), f ($f = (n^2+3)/3$; n is the refractive index obtained by using eq. 15) is the local field correction factor with respect to Lorentz expression, N is the number of molecules per unit cm^3 , $\bar{\alpha}$ obtained by using eq. 2 is the theoretical linear optical polarizability, and so the $\chi^{(1)}$ parameter is calculated by using the eq. (16).

Likewise, the third-order nonlinear optical susceptibility $\chi^{(3)}$ associated with the γ parameter without using the experimental technique was obtained by using the eq. (17) [29,84].

$$\chi^{(3)} = Nf^4\gamma \quad (17)$$

In eq. (17), N and f is defined above. γ is the second-hyperpolarizability calculated by using eq. (5).

The HSEh1PBE level within the gas phase and ethanol solvent was applied to examine the refractive index, linear optical polarizability, second- and third-order nonlinear optical parameters of the complexes **1** and **2**. The obtained theoretical results were compared with p-nitroaniline (pNA) [85], nitrobenzene [86], TFMB [84] and urea [87,88]. Calculated μ , α , $\Delta\alpha$, n , $\chi^{(1)}$, β , γ and $\chi^{(3)}$ parameters were presented in Table 4. The n values of the complexes **1** and **2** were experimentally obtained at 1.39 and 1.26, and calculated at 1.45 and 1.40 in the gas phase by using HSEh1PBE level, respectively. These results are remarkably coherent. The linear response α and $\chi^{(1)}$ parameters as a measure of polarization susceptibility for the complexes **1** and **2** in the gas phase were found to be 45.2×10^{-24} , 20.58×10^{-24} esu and 29.5×10^{-24} , 14.75×10^{-24} , respectively. These results are comparable to previous ones [28,29]. Moreover, the α values of the complex **1** found to have larger values than all chalcones derivative obtained at the range from 27 to 39.3×10^{-24} [78].

The second-order NLO β values of the complex **1** in ethanol solvent and the gas phase were found to be 55.3×10^{-30} and 30.9×10^{-30} esu, and these values were obtained at 425.38/6.01 and 237.69/3.36 times higher than those of urea (0.130×10^{-30} esu) [88]/pNA (9.2×10^{-30} esu) [85], respectively. Furthermore, the calculated β values of the complex **1** were found as larger than some chalcones derivative calculated at 19.7 - 31.9×10^{-30} esu [78] while these values of the complex **1** were calculated the lower than those of 4NH₂-Chalcone and 4NO₂-CH₃-Chalcone found at 67.7 and 64.8×10^{-30} esu [78]. From these results, the role on NLO parameters of the different substitutions and metal ions compounds was clearly observed. The third-order NLO γ values of the complex **1** in ethanol solvent and gas phase calculated at 251.0×10^{-36} and 110.2×10^{-36} esu are 16.73 and 7.33 times higher than that of pNA (15×10^{-36} esu). The γ results were also supported by the third-order nonlinear optical susceptibility $\chi^{(3)}$ parameter obtained at 119.47×10^{-13} and 25.80×10^{-13} esu values. The differences between NLO parameters of these complexes are originated from the coordination environment and the effect of symmetry center on metal ions. It could be considered that the presence of Cr metal ion and its coordination environment increased the NLO activity of the complex **1**, which is bulkier than the complex **2**, despite the fact that the atomic diameter of V metal is larger than that of Cr metal.

According to the results of second- and third-order β and γ parameters in gas the phase and ethanol solvent, it is concluded that complex **1** could be a material efficient for microscopic second-order and third-order NLO property.

3.5. α -Glucosidase activity and molecular docking

The complexes **1** and **2** were screened for the α -glucosidase inhibition. The IC₅₀ values of the complexes **1** and **2**, acarbose, genistein and resveratrol [89-92], well-known as α -glucosidase inhibitors, are comparatively given in Table 6. IC₅₀ values of the complexes **1** and **2** against α -glucosidase were found to be >600 μ M.

According to the structure-activity relationship (SAR), the following points could be concluded from Table 6:

- (i) It could be concluded that the IC_{50} values of the complexes **1** and **2** did not defect on coordination environment and the metal ions in coordination.
- (ii) The inhibitory activity ($IC_{50} = >600 \mu M$) of the complex **1** is the same as previously synthesized Cr(III) complex of mixed-ligand (6-mpa with NCS) [17] despite differences in the coordination environment of these complexes.
- (iii) The coordination geometries around Cr(III) and V(IV) ions of the complexes **1** and **2** determined as distorted octahedral geometry and square-bipyramidal did not show a remarkable effect on α -glucosidase inhibition. Furthermore, even if it could be considered the atomic diameter of V metal is larger than the Cr metal and but Cr complex is bulkier than the V complex, the complexes **1** and **2** did not demonstrate a remarkable effect on α -glucosidase inhibition at the μM level.

To date, the IC_{50} values of metal complexes including 3-mpa ligand have been not reported. But the α -glucosidase activity studies of synthesized mixed-ligand metal complexes containing 6-mpa ligand were performed [16-20]. Obtained the IC_{50} values are similar to previously reported results.

In order to investigate the interactions binding site of the target protein (the template structure *S. cerevisiae* isomaltase (PDBID: 3A4A)) with the complexes **1** and **2**, molecular docking study was fulfilled by using the iGEMDOCK program [93]. The estimated interactions and their energy values for the complexes **1** and **2** were tabulated in Table 6. Fig. S3 demonstrates the interacting of the complexes **1** and **2** with amino-acid residues thanks to some hydrogen-bonding and van der Waals interactions. Based on docking results, the E_{tot} of the complexes **1** and **2** were obtained at -107.3 and -97.0 kcal/mol, respectively. These energies include the interactions of same or different amino-acid residues with the complexes **1** and **2**.

The H-bonding interactions for complex **1** obtained at -5.2, -8.6 and -2.7 kcal/mol were determined between carbonyl oxygen atom of 3-mpa ligand and the S (side chain)-SER240/ASP242 O^{γ}/O^{δ} (with 2.82 and 2.79 Å bond distances) and M (main chain)-ARG315 N^{α} (with 3.21 Å bond distance). These interactions are similar to previously synthesized Cr(III) complex of mixed-ligand (6-mpa with NCS) in spite of despite differences in the coordination environment of these complexes. Likewise, the H-bonding interactions for complex **2** calculated at -6.5 and -5.0 kcal/mol were defined between the M-SER298 N^{α} (with 2.95 Å bond distance)/S-SER298 O^{γ} (with 2.69 Å bond distance) and carbonyl oxygen atom of 3-mpa.

In summary, it is said that these differences could be stem from the coordination environment and the metal ions in coordination for these complexes.

4. Conclusion

The complexes **1** and **2** {[Cr(3-mpa)₃], (**1**), [VO(3-mpa)₂], (**2**)} were synthesized and characterized by XRD and LC-MS/MS methods. FT-IR and UV-Vis spectral analysis were utilized to examine their spectral properties. So as to interpret the corresponding detailed experimental spectral properties results, theoretical calculations were performed by using HSEh1PBE/6-311G(d,p)/LanL2DZ level. Moreover, the $n \rightarrow \pi^*$ and $\pi \rightarrow \pi^*$ transitions for the complexes **1** and **2** in ethanol solvent observed at 270 and 218, 273 and 210 nm were determined by TD/DFT calculations, these transitions were originated from inter-ligand and intra-ligand charge transfer interactions. It could be concluded that the substantial absorption peaks of the complexes **1** and **2** in ethanol solvent observed at 321 and 371 nm originated between metal–ligand and ligand–ligand charge transfer with the electronic contributions of $H \rightarrow L + 3\alpha (+48\%) // Cr (61\%) + 3-Mepy (27\%) + COO^- (12\%) \rightarrow Cr (11\%) + 3-Mepy (77\%) + COO^- (12\%)$ for the complex **1** and $H \rightarrow L\alpha (+77\%) // VO (59\%) + 3-$

Mepy(23%)+COO⁻(18%)→VO(7%)+3-Mepy(80%)+COO⁻(13%) for the complex **2**. NBO results verify the coordination environments for the complexes **1** and **2** depicted by n→n* interactions due to the delocalization effect observed between lone-pair (n) orbitals of nitrogen/oxygen atom and anti-lone-pair (n*) orbitals of Cr(III) and V(IV) ions. NLO studies demonstrate that the complex **1** is a promising candidate to materials with high values of nonlinear parameters (β , γ and $\chi^{(3)}$) calculated at 55.3×10^{-30} , 251.0×10^{-36} and 119.47×10^{-13} esu in ethanol solvent. Considering all theoretical and experimental results, it stands out as a good coherent between the theoretical and corresponding experimental results. The IC₅₀ values of α -glucosidase inhibition for the synthesized complexes **1** and **2** were obtained at >600 μ M. It can be said that these complexes did not display a significant effect on α -glucosidase inhibition at μ M level. In brief, it could be stated that the NLO and in vitro results provide useful information for mixed-ligand metal complexes including 3-mpa and its derivatives to be synthesized.

Acknowledgements

This work was supported by the Scientific and Technological Research Council of Turkey (TÜBİTAK) (Project Number: MFAG-117F235).

References

- [1] E.C. Constable, P.J. Steel, N,N'-Chelating biheteroaromatic ligands; a survey, *Coord. Chem. Rev.* 93 (1989) 205–223.
- [2] H. Adams, N.A. Bailey, J.D. Crane, D.E. Fenton, J.M. Latour, J.M. Williams, Manganese (II) and iron (III) complexes of the tridentate ligands bis (benzimidazol-2-ylmethyl)-amine (L₁) and -methylamine (L₂). Crystal structures of [MnL₁(CH₃CO₂)₂], [FeL₂Cl₃], and [Fe₂L₁₂(μ -O){ μ -(CH₃)₃CCO₂}₂][ClO₄]₂, *J. Chem. Soc., Dalton Transactions*, 5 (1990) 1727–1735.
- [3] W.L. Driessen, R.A.G. De Graaff, F.J. Parlevliet, J. Reedijk, R.M. De Vos, Transition metal compounds of the tridentate pyrazole substituted amine ligand bis (2-(3,5-dimethyl-1-pyrazolyl) ethyl) ethylamine (ddae). X-ray structures of [Co(ddae)(NO₃)₂], [Cu(ddae)(NO₃)(H₂O)](NO₃) and [Cu(ddae)(Cl)₂]·C₂H₅OH, *Inorg. Chim. Acta* 216(1) (1994) 43–49.
- [4] F. Grob, A. Müller-Hartmann, H. Vahrenkamp, Diphosphate- Zinc Complexes with Tridentate Coligands, *Eur. J. Inorg. Chem.* 2000(11) (2000) 2363–2370.
- [5] M. Gollapalli, M. Taha, M.T. Javid, N.B. Almandil, F. Rahim, A. Wadood, A. Mosaddik, M. Ibrahim, M.A. Alqahtani, Y.A. Bamarouf, Synthesis of benzothiazole derivatives as a potent α -glucosidase inhibitor, *Bioorg. Chem.* 85 (2019) 33–48.
- [6] U. Ghani, Re-exploring promising α -glucosidase inhibitors for potential development into oral anti-diabetic drugs: Finding needle in the haystack, *Eur. J. Med. Chem.* 103 (2015) 133–162.
- [7] K.D. Demadis, S.D. Katarachia, Metal-phosphonate chemistry: Synthesis, crystal structure of calcium-amino tris- (methylene phosphonate) and inhibition of CaCO₃ crystal growth, *Phosphorus, Sulfur, and Silicon*, 179(3) (2004) 627–648.
- [8] J.G. Mao, Structures and luminescent properties of lanthanide phosphonates, *Coord. Chem. Rev.* 251(11) (2007) 1493–1520.
- [9] J. Monot, M. Petit, S.M. Lane, I. Guisle, J. Léger, C. Tellier, D.R. Talham, B. Bujoli, Towards zirconium phosphonate-based microarrays for probing DNA- protein interactions: Critical influence of the location of the probe anchoring groups, *J. Am. Chem. Soc.* 130(19) (2008) 6243–6251.

- [10] A.M. Hardy, R.L. LaDuca, Synthesis and structure of a cobalt dicyanamide chain coordination polymer incorporating a long-spanning hydrogen-bonding capable diimine with a novel binodal (4,6)-connected supramolecular topology, *Inorg. Chem. Comm.* 12(4) (2009) 308–311.
- [11] J. Umeda, M. Suzuki, M. Kato, M. Moriya, W. Sakamoto, T. Yogo, Proton conductive inorganic-organic hybrid membranes functionalized with phosphonic acid for polymer electrolyte fuel cell, *J. Power Sources* 195(18) (2010) 5882–5888.
- [12] S. Adisakwattana, P. Charoenlertkul, S. Yibchok-Anun, α -Glucosidase inhibitory activity of cyanidin-3-galactoside and synergistic effect with acarbose, *J. Enzym. Inhib. Med. Chem.* 24(1) (2009) 65–69.
- [13] J.L. Chiasson, R.G. Josse, R. Gomis, M. Hanefeld, A. Karasik, M. Laakso, STOP-NIDDM trial research group. Acarbose for the prevention of Type 2 diabetes, hypertension and cardiovascular disease in subjects with impaired glucose tolerance: Facts and interpretations concerning the critical analysis of the STOPNIDDM Trial data, *Lancet*, 359 (2002) 2072–2077.
- [14] C.M.M. Santos, M. Freitas, E. Fernandes, A comprehensive review on xanthone derivatives as α -glucosidase inhibitors, *Eur. J. Med. Chem.* 157 (2018) 1460–1479.
- [15] Y. Yoshikawa, R. Hirata, H. Yasui, H. Sakurai, Alpha-glucosidase inhibitory effect of anti-diabetic metal ions and their complexes, *Biochimie* 91 (2009) 1339–1341.
- [16] E. Ueda, Y. Yoshikawa, H. Sakurai, Y. Kojima, N.M. Kajiwara, In vitro α -glucosidase inhibitory effect of Zn(II) complex with 6-methyl-2-picolinmethylamide, *Chem. Pharm. Bull.* 53(4) (2005) 451–452.
- [17] D. Avcı, S. Altürk, F. Sönmez, Ö. Tamer, A. Başoğlu, Y. Atalay, B.Z. Kurt, N. Dege, Three novel Cu(II), Cd(II) and Cr(III) complexes of 6-Methylpyridine-2-carboxylic acid with thiocyanate: Synthesis, crystal structures, DFT calculations, molecular docking and α -Glucosidase inhibition studies, *Tetrahedron* 74 (2018) 7198–7208.
- [18] D. Avcı, S. Altürk, F. Sönmez, Ö. Tamer, A. Başoğlu, Y. Atalay, B.Z. Kurt, N. Dege, A novel series of M(II) complexes of 6-methylpyridine-2-carboxylic acid with 4(5) methylimidazole: Synthesis, crystal structures, α -glucosidase activity, density functional theory calculations and molecular docking. *Appl. Organometal. Chem.* (2019) e4935.
- [19] D. Avcı, S. Altürk, F. Sönmez, Ö. Tamer, A. Başoğlu, Y. Atalay, B. Zengin Kurt, N. Dege, A novel series of mixed-ligand M(II) complexes containing 2,2'-bipyridyl as potent α -glucosidase inhibitor: synthesis, crystal structure, DFT calculations, and molecular docking, *JBIC J. Biol. Inorg. Chem.* 24 (2019) 747–764.
- [20] D. Avcı, S. Altürk, F. Sönmez, Ö. Tamer, A. Başoğlu, Y. Atalay, B. Zengin Kurt, N. Dege, Novel Cu(II), Co(II) and Zn(II) metal complexes with mixed-ligand: Synthesis, crystal structure, α -glucosidase inhibition, DFT calculations, and molecular docking, *J. Mol. Struct.* 1197 (2019) 645–655.
- [21] B.-M. Kukovec, I. Kodrin, V. Vojković, Z. Popović, Synthesis, X-ray structural, IR spectroscopic, thermal and DFT studies of nickel(II) and copper(II) complexes with 3-methylpicolinic acid. UV-Vis spectrophotometric study of complexation in the solution, *Polyhedron* 52 (2013) 1349–1361.
- [22] B.-M. Kukovec, Z. Popović, Š. Komorsky-Lovrić, V. Vojković, M. Vinković, Synthesis, structural, spectroscopic and thermal characterization of cobalt complexes with 3- and 6-methylpicolinic acid. Voltammetric and spectrophotometric study in solution, *Inorg. Chim. Acta* 362 (2009) 2704–2714.
- [23] B.-M. Kukovec, Z. Popović, G. Povlović, Synthesis and characterization of copper(II) complexes with 3-methylpicolinic acid. Crystal and molecular structure of *bis*(3-methylpicolinato-*N,O*)(4-picoline)copper(II), *J. Coord. Chem.* 61(19) (2008) 3092–3101.

- [24] J. W. Lai, C.W. Chan, C.H. Ng, I.H. Ooi, K.W. Tan, M.J. Maah, S.W. Ng, Hydrated and anhydrous forms of copper(II) complex of 3-methylpicolinic acid, and spectroscopic studies of their ROS-inducing and proteasome inhibition, *J. Mol. Struct.* 1106 (2016) 234–241.
- [25] A. Rana, S.K. Jana, S. Datta, R.J. Butcher, E. Zangrando, S. Dalai, 1D coordination polymers formed by tetranuclear lead(II) building blocks with carboxylate ligands: In situ isomerization of itaconic acid, *J. Solid State Chem.* 207 (2013) 61–68.
- [26] E. L-Chruscinska, G. Micera, and E. Garribba, Complex Formation in Aqueous Solution and in the Solid State of the Potent Insulin-Enhancing $V^{IV}O^{2+}$ Compounds Formed by Picolinate and Quinolate Derivatives, *Inorg. Chem.* 50 (2011) 883–899].
- [27] A. A. Baroud, L.E. Mihajlović-Lalić, N. Gligorijević, S. Arandelović, D. Stanković, S. Radulović, K. Van Hecke, A. Savić and S. Grgurić-Šipka, Ruthenium(II) bipyridine complexes: from synthesis and crystal structures to electrochemical and cytotoxicity investigation *J. Coord. Chem.* 70(5) (2017) 831–847.
- [28] S. Altürk, D. Avcı, A. Başoğlu, Ö. Tamer, Y. Atalay, N. Dege, Copper(II) complex with 6-methylpyridine-2-carboxylic acid: Experimental and computational study on the XRD, FT-IR and UV–Vis spectra, refractive index, band gap and NLO parameters, *Spectrochim. Acta A* 190 (2018) 220–230.
- [29] S. Altürk, D. Avcı, Ö. Tamer, Y. Atalay, O. Şahin, A cobalt(II) complex with 6-methylpicolinate: synthesis, characterization, second- and third-order nonlinear optical properties, and DFT calculations, *J. Phys. Chem. Solids* 98 (2016) 71–80.
- [30] Q.-X. Wu, Y. Geng, Y. Liao, X.-Dan Tang, G.-Chun Yang, Z.-Min Su, Theoretical studies of the effect of electron-withdrawing dicyanovinyl group on the electronic and charge-transport properties of fluorene-thiophene oligomers. *Theor. Chem. Acc.* 131 (2012) 1121.
- [31] S. Altürk, Ö. Tamer, D. Avcı, Y. Atalay, Synthesis, spectroscopic characterization, second and third-order nonlinear optical properties, and DFT calculations of a novel Mn(II) complex. *J. Organomet. Chem.* 797 (2015) 110–119.
- [32] F. Castet, V. Rodriguez, J.-L. Pozzo, L. Ducasse, A. Plaquet, B. Champagne, Design and Characterization of Molecular Nonlinear Optical Switches. *Acc. Chem. Res.* 46 (2013) 2656–2665.
- [33] L.E. Johnson, L.R. Dalton and B.H. Robinson, Optimizing Calculations of Electronic Excitations and Relative Hyperpolarizabilities of Electrooptic Chromophores. *Acc. Chem. Res.* 47 (2014) 3258–3265.
- [34] K. Garrett, X.A.S. Vazquez, S.B. Egri, J. Wilmer, L.E. Johnson, B.H. Robinson, C.M. Isborn, Optimum Exchange for Calculation of Excitation Energies and Hyperpolarizabilities of Organic Electro-optic Chromophores. *J. Chem. Theory Comput.* 10 (2014) 3821–3831.
- [35] R. S. Roy and P.K. Nandi, Exploring bridging effect on first hyperpolarizability, *RSC Adv.* 5 (2015) 103729–103738.
- [36] M.U. Khan, M. Khalid, M. Ibrahim, A.A.C. Braga, M. Safdar, A.A. Al-Saadi, M.R.S.A. Janjua, First Theoretical Framework of Triphenylamine–Dicyanovinylene-Based Nonlinear Optical Dyes: Structural Modification of π -Linkers, *J. Phys. Chem. C* 122(7) (2018) 4009–4018.
- [37] M.U. Khan, M. Ibrahim, M. Khalid, M.S. Qureshi, T. Gulzar, K.M. Zia, A.A. Al-Saadi, M.R.S.A. Janjua, First theoretical probe for efficient enhancement of nonlinear optical properties of quinacridone based compounds through various modifications, *Chem. Phys. Lett.* 715 (2019) 222–230.
- [38] M.U. Khan, M. Ibrahim, M. Khalid, A.A.C. Braga, S. Ahmed, A. Sultan, Prediction of Second-Order Nonlinear Optical Properties of D– π –A Compounds Containing Novel Fluorene Derivatives: A Promising Route to Giant Hyperpolarizabilities, *J. Clust. Sci.* 30(2) (2019) 415–430.

- [39] M.U. Khan, M. Ibrahim, M. Khalid, S. Jamil, A.A. Al-Saadi, M.R.S.A. Janjua, Quantum chemical designing of indolo[3,2,1-jk]carbazole-based dyes for highly efficient nonlinear optical properties, *Chem. Phys. Lett.* 719 (2019) 59-66.
- [40] M.R.S.A. Janjua, M. Amin, M. Ali, B. Bashir, M.U. Khan, M.A. Iqbal, W. Guan, L. Yan, Z.-M. Su, A DFT Study on The Two-Dimensional Second-Order Nonlinear Optical (NLO) Response of Terpyridine-Substituted Hexamolybdates: Physical Insight on 2D Inorganic–Organic Hybrid Functional Materials, *Eur. J. Inorg. Chem.* 2012(4) (2012) 705-711.
- [41] M.R.S.A. Janjua, M.U. Khan, B. Bashir, M.A. Iqbal, Y. Song, S.A.R. Naqvi, Z.A. Khan, Effect of π -conjugation spacer ($-\text{C}\equiv\text{C}-$) on the first hyperpolarizabilities of polymeric chain containing polyoxometalate cluster as a side-chain pendant: A DFT study, *Comput. Theor. Chem.* 994 (2012) 34-40
- [42] J.L. Oudar, Optical nonlinearities of conjugated molecules. Stilbene derivatives and highly polar aromatic compounds. *J. Chem. Phys.* 67 (1977) 446–457.
- [43] D. Avcı, The consistency analysis of different semiempirical calculations on second- and third-order nonlinear optical properties of donor–acceptor chromophores containing α -cyan *Spectrochim. Acta A* 77 (2010) 665–672.
- [44] D. Avcı, Second and third-order nonlinear optical properties and molecular parameters of azo chromophores: Semiempirical analysis. *Spectrochim. Acta A* 82 (2011) 37–43.
- [45] J.L. Oudar, J. Zyss, Relations between microscopic and macroscopic lowest-order optical nonlinearities of molecular crystals with one-or two-dimensional units. *Phys. Rev. A* 26 (1982) 2028–2048.
- [46] Y. Zhang, C.-Y. Zhao, W.-H. Fang, X.-Z. You, Theor. A molecular design view on the first hyperpolarizability of salicylideneaniline derivatives. *Chem. Acc.* 96 (1997) 129–134.
- [47] D. Avcı, Ö. Tamer, Y. Atalay, Solvatochromic effect on UV–vis absorption and fluorescence emission spectra, second- and third-order nonlinear optical properties of dicyanovinyl-substituted thienylpyrroles: DFT and TDDFT study, *J. Mol. Liq.* 220 (2016) 495–503.
- [48] J.O. Morley, Theoretical Study of the Electronic Structure and Hyperpolarizabilities of Donor-Acceptor Cumulenes and a Comparison with the Corresponding Polyenes and Polyynes. *J. Phys. Chem.* 99 (1995) 10166–10174.
- [49] S. Altürk, D. Avcı, Ö. Tamer, Y. Atalay, Comparison of different hybrid DFT methods on structural, spectroscopic, electronic and NLO parameters for a potential NLO material, *Comput. Theor. Chem.* 1100 (2017) 34–45
- [50] Mohd. Shkir, Investigation on the key features of L-Histidinium 2-nitrobenzoate (LH2NB) for optoelectronic applications: A comparative study, *J. King Saud Univ. Sci.* 29 (2017) 70-83.
- [51] S.R. Maidur, P.S. Patil, S.V. Rao, M. Shkir, S.M. Dharmaprakash, Experimental and computational studies on second-and third-order nonlinear optical properties of a novel D- π -A type chalcone derivative: 3-(4-methoxyphenyl)-1-(4-nitrophenyl) prop-2-en-1-one, *Opt Laser Technol* 97 (2017) 219–228.
- [52] Mohd. Shkir, P.S. Patil, M. Arora, S. AlFaify, H. Algarni, An experimental and theoretical study on a novel donor- π -acceptor bridge type 2, 4, 5-trimethoxy-4'-chlorochalcone for optoelectronic applications: A dual approach, *Spectrochim. Acta A* 173 (2017) 445–456.
- [53] J. Chai, Y. Liu, J. Dong, B. Liu, B. Yang, Synthesis, structure, chemical and bioactivity behavior of eight chromium(III) picolinate derivatives $\text{Cr}(\text{R-pic})_3$, *Inorg. Chim. Acta* 466 (2017) 151–159.
- [54] G.M. Sheldrick, SHELXT – integrated space-group and crystal-structure determination, *Acta Cryst A* 71 (2015) 3–8.
- [55] C.F. Macrae, P.R. Edgington, P.McCabe, E. Pidcock, G.P. Shields, R. Taylor, M. Towler,

- J. van de Streek, Mercury Visualization and Analysis of Crystal Structures, *J. Appl. Crystallogr.* 39 (2006) 453–457.
- [56] A.L. Spek, Structure validation in chemical crystallography, *Acta Cryst. D65* (2009) 148–155.
- [57] M.J. Frisch, G.W. Trucks, H.B. Schlegel, G.E. Scuseria, M.A. Robb, J.R. Cheeseman, G. Scalmani, V. Barone, B. Mennucci, G.A. Petersson, H. Nakatsuji, M. Caricato, X. Li, H.P. Hratchian, A.F. Izmaylov, J. Bloino, G. Zheng, J.L. Sonnenberg, M. Hada, M. Ehara, K. Toyota, R. Fukuda, J. Hasegawa, M. Ishida, T. Nakajima, Y. Honda, O. Kitao, H. Nakai, T. Vreven, J.A. Montgomery Jr., J.E. Peralta, F. Ogliaro, M. Bearpark, J.J. Heyd, E. Brothers, K.N. Kudin, V.N. Staroverov, R. Kobayashi, J. Normand, K. Raghavachari, A. Rendell, J.C. Burant, S.S. Iyengar, J. Tomasi, M. Cossi, N. Rega, J.M. Millam, M. Klene, J.E. Knox, J.B. Cross, V. Bakken, C. Adamo, J. Jaramillo, R. Gomperts, R.E. Stratmann, O. Yazyev, A.J. Austin, R. Cammi, C. Pomelli, J.W. Ochterski, R.L. Martin, K. Morokuma, V.G. Zakrzewski, G.A. Voth, P. Salvador, J.J. Dannenberg, S. Dapprich, A.D. Daniels, O. Farkas, J.B. Foresman, J.V. Ortiz, J. Cioslowski, D.J. Fox, Gaussian 09, Revision D.01, Gaussian, Inc., Wallingford, CT, 2013.
- [58] R. Dennington, T. Keith, J. Millam, GaussView, Version 5, Semichem Inc., Shawnee Mission KS, 2009.
- [59] J. Heyd, G.E. Scuseria, Efficient hybrid density functional calculations in solids: assessment of the Heyd-Scuseria-Ernzerhof screened Coulomb hybrid functional, *J. Chem. Phys.* 121 (2004) 1187–1192.
- [60] A.V. Krukau, O.A. Vydrov, A.F. Izmaylov, G.E. Scuseria, Influence of the exchange screening parameter on the performance of screened hybrid functionals, *J. Chem. Phys.* 125 (2006) 224106.
- [61] M.J. Frisch, J.A. Pople, J.S. Binkley, Self-consistent molecular orbital methods 25. Supplementary functions for Gaussian basis set, *J. Chem. Phys.* 80 (1984) 3265–3269.
- [62] P.J. Hay, W.R. Wadt, Ab initio effective core potentials for molecular calculations. Potentials for the transition metal atoms Sc to Hg, *J. Chem. Phys.* 82 (1985) 270–283.
- [63] E.D. Glendening, A.E. Reed, J.E. Carpenter, F. Weinhold, NBO Version 3.1, TCI, University of Wisconsin, Madison, 1998.
- [64] A.E. Reed, F. Weinhold, Natural bond orbital analysis of near-Hartree-Fock water dimer, *J. Chem. Phys.* 78 (1983) 4066–4073.
- [65] J.P. Foster, F. Weinhold, Natural hybrid orbitals, *J. Am. Chem. Soc.* 102 (1980) 7211–7218.
- [66] E. Runge, E.K.U. Gross, Density-functional theory for time-dependent systems, *Phys. Rev. Lett.* 52 (1984) 997–1000.
- [67] S. Miertus, E. Scrocco, J. Tomasi, Electrostatic interaction of a solute with a continuum. A direct utilization of Ab initio molecular potentials for the prevision of solvent effects, *J. Chem. Phys.* 55 (1981) 117–129.
- [68] W. Yang, R.G. Parr, Hardness, softness, and the Fukui function in the electronic theory of metals and catalysis, *Proc. Natl. Acad. Sci. USA* 82 (1985) 6723–6726.
- [69] S.I. Gorelsky, SWizard Program Revision 4.5, University of Ottawa, Ottawa, Canada, 2010 <http://www.sg.chem.net/>.
- [70] L. Skripnikov, Chemissian: software to analyze spectra, build density maps and molecular orbitals, Version 4 (43) (2016).
- [71] İ. Şişman, A. Başoğlu, Effect of Se content on the structural, morphological and optical properties of Bi₂Te_{3-y}Se_y thin films electrodeposited by under potential deposition technique, *Mater. Sci. Semicond. Process.* 54 (2016) 57–64.

- [72] J. Spöner, P. Hobza, DNA base amino groups and their role in molecular interactions: Ab initio and preliminary density functional theory calculations, *Int. J. Quantum Chem.* 57 (1996) 959–970.
- [73] S.R. Gadre, I.H. Shrivastava, Shapes and sizes of molecular anions via topographical analysis of electrostatic potential, *J. Chem. Phys.* 94 (1991) 4384–4390.
- [74] Mohd. Shkir, S. AlFaify, M. Arora, V. Ganesh, H. Abbas, I.S. Yahia, A first principles study of key electronic, optical, second and third order nonlinear optical properties of 3-(4-chlorophenyl)-1-(pyridin-3-yl) prop-2-en-1-one: a novel D- π -A type chalcone derivative, *J. Comput. Electron* 17 (2018) 9-20.
- [75] S. AlFaify, Mohd. Shkir, M. Arora, A. Irfan, H. Algarni, H. Abbas, A.G. Al-Sehemi, Quantum chemical investigation on molecular structure, vibrational, photophysical and nonlinear optical properties of L-threoninium picrate: an admirable contender for nonlinear applications, *J. Comput. Electron* 17 (2018) 1421-1433.
- [76] Mohd. Shkir, A. Irfan, S. AlFaify, P.S. Patil, A.G. Al-Sehemi, Linear, second and third order nonlinear optical properties of novel noncentrosymmetric donor-acceptor configure chalcone derivatives: A dual approach study, *Optik* 199 (2019) 163354.
- [77] Mohd. Shkir, S. Muhammad, S. AlFaify, A.R. Chaudhry, A.G. Al-Sehemi, Shedding light on molecular structure, spectroscopic, nonlinear optical and dielectric properties of bis(thiourea) silver(I) nitrate single crystal: A dual approach, *Arab. J. Chem.* 12 (2019) 4612–4626.
- [78] S. Omara, Mohd. Shkir, M.A. Khan, Z. Ahmad, S. AlFaify, A comprehensive study on molecular geometry, optical, HOMO-LUMO, and nonlinear properties of 1,3-diphenyl-2-propen-1-ones chalcone and its derivatives for optoelectronic applications: A computational approach, *Optik* 204 (2020) 164172.
- [79] M.-S. Bahae, A.A. Said, T.-H. Wei, D.J. Hagan, E.W.V. Stryland, Sensitive measurement of optical nonlinearities using a single beam, *IEEE J. Quantum Electron.* 26 (1990) 760–769.
- [80] Y. Qian, G. Xiao, G. Wang, Y. Sun, Y. Cui, C. Yuan, Synthesis and third-order optical nonlinearity in two-dimensional A- π -D- π -A carbazole-cored chromophores, *Dyes Pigments* 71 (2006) 109–117.
- [81] Y. Qian, G. Xiao, G. Wang, B. Lin, Y. Cui, Y. Sun, Synthesis and Z-scan measurements of third-order optical nonlinearity in push-pull molecules with dihydroxyethyl amino donor and nitro acceptor, *Dyes Pigments* 75 (2007) 218–224.
- [82] C. An, X. Feng, N. Zhao, P. Liu, T. Wang, Z. Lian, Syntheses, structures and third-order nonlinear optical properties of two-dimensional rhombohedral grid coordination polymers: $[\text{Cd}(\text{imz})_3]_2(\text{BTC}) \cdot 0.5\text{H}_2\text{O}$ and $[\text{Cu}_4(\text{H}_2\text{O})_2(\text{imz})_8](\text{BTC})_2 \cdot 7\text{H}_2\text{O}$ (BTC = 1, 2, 4, 5-benzenetetracarboxylate anion, imz = imidazole), *J. Clust. Sci.* 26 (2015) 889–900.
- [83] M.-T. Zhao, B.P. Singh, P.N. Prasad, A systematic study of polarizability and microscopic third-order optical nonlinearity in thiophene oligomers, *J. Chem. Phys.* 89 (1988) 5535–5541.
- [84] D. Avcı, S. Altürk, Ö. Tamer, M. Kuşbazoğlu, Y. Atalay, Solvent effect in implicit/explicit model on FT-IR, ^1H , ^{13}C and ^{19}F NMR, UV-vis and fluorescence spectra, linear, second- and third-nonlinear optical parameters of 2-(trifluoromethyl)benzoic acid: Experimental and computational study, *J. Mol. Struct.* 1143 (2017) 116–126.
- [85] L.-T. Cheng, W. Tam, S.H. Stevenson, G.R. Meredith, G. Rikken, S.R. Marder, Experimental investigations of organic molecular nonlinear optical polarizabilities. 1. Methods and results on benzene and stilbene derivatives, *J. Phys. Chem.* 95 (1991) 10631–10643.

- [86] K.D. Singer, A.F. Garito, Measurements of molecular second order optical susceptibilities using dc induced second harmonic generation, *J. Chem. Phys.* 75 (1981) 3572–3580.
- [87] I. Ledoux, J. Zyss, Influence of the molecular environment in solution measurements of the second-order optical susceptibility for urea and derivatives, *Chem. Phys.* 73 (1982) 203–213.
- [88] C. Adant, M. Dupuis, J.L. Bredas, Ab initio study of the nonlinear optical properties of urea: electron correlation and dispersion effects, *Int. J. Quantum Chem.* 56 (2004) 497–507.
- [89] M. Taha, N. Hadiani Ismail, S. Lalani, M. Qaiser Fatmi, Atia-tul-Wahab, S. Siddiqui, K.M. Khan, S. Imran, M. Iqbal Choudhary, Synthesis of novel inhibitors of α -glucosidase based on the benzothiazole skeleton containing benzohydrazide moiety and their molecular docking studies, *Eur. J. Med. Chem.* 92 (2015) 387–400.
- [90] M. Taha, N. Hadiani Ismail, M. Syukri Baharudin, S. Lalani, S. Mehboob, K.M. Khan, S. Yousuf, S. Siddiqui, F. Rahim, M.I. Choudhary, Synthesis crystal structure of 2-methoxybenzoylhydrazones and evaluation of their α -glucosidase and urease inhibition potential, *Med. Chem. Res.* 24 (2015) 1310–1324.
- [91] J.-W. Zheng, L. Ma, Silver(I) complexes of 2,4-dihydroxybenzaldehyde–amino acid Schiff bases–Novel noncompetitive α -glucosidase inhibitors, *Bioorg. Med. Chem. Lett.* 25 (2015) 2156–216.
- [92] J.-W. Zheng, L. Ma, Metal complexes of anthranilic acid derivatives: A new class of non-competitive α -glucosidase inhibitors, *Chin. Chem. Lett.* 27 (2016) 627–630.
- [93] J.-M. Yang, C.-C. Chen, GEMDOCK: a generic evolutionary method for molecular docking, *Proteins* 55 (2004) 288–304.

Table 1. Crystal data and structure refinement parameters for the complex **1**.

CCDC Number	1588068
Empirical formula	C ₂₁ H ₁₈ CrN ₃ O ₆
Formula weight	460.38
Crystal system	Monoclinic
Space group	C2/c
Temperature (K)	296
Radiation type	Mo K α
λ (Å)	0.71073
Crystal size (mm)	0.55x0.42x0.21
Crystal shape and colour	Prism and red
a (Å)	31.7393 (19)
b (Å)	8.5310 (6)
c (Å)	14.8857 (10)
α (°)	90
β (°)	96.720 (5)
γ (°)	90
V (Å ³)	4002.9 (5)
Z	8
F(000)	1896
Density (Mg m ⁻³)	1.528
μ (mm ⁻¹)	0.62
θ range (°)	1.8–28.5
<i>h</i> , <i>k</i> , <i>l</i>	–38→30, –10→10, –18→18
Measured refls.	10348
Independent refls.	3933
R _{int}	0.042
R[F ² > 2 σ (F ²)], wR(F ²), S	0.041, 0.102, 0.92
max/min (e Å ⁻³)	0.35/–0.21

Table 2. Hydrogen-bond parameters for complex **1** (Å and °).

D-H...A	D-H	H...A	D...A	D-H...A
C14-H14A...O4	0.96	2.11	2.876 (5)	136
C6-H6...O4 ⁱ	0.93	2.31	3.045 (4)	135
C20-H20...O6 ⁱⁱ	0.93	2.38	3.125 (3)	137

Symmetry codes: (i) $-x+1, -y+1, -z+1$; (ii) $x, -y+1, z+1/2$.

Table 3. Comparison of the FT-IR and calculated vibrational frequencies for the complexes **1** and **2**.

Assignments	Complex 1		Complex 2	
	FT-IR	HSEh1PBE	FT-IR	HSEh1PBE
ν CH	3105	3106	3097	3106
ν CH	3092	3091		3065
ν CH	3064	3067		
ν CH	3007	3017	2989	3017
ν CH		3015		3017
ν CH ₃	2993	2944	2933	2944
ν CH ₃	2937	2943	2900	2944
ν_{as} COO ⁻	1665	1741	1627	1741
ν C=C + ν N=C	1640	1588		
ν C=C	1586	1586	1585	1586
β HCC	1453	1443	1456	1442
β HCH	1417	1438	1358	1359
ν NC + ν OC	1315	1309		
ν NC	1189	1199	1280	1315
ν_s COO ⁻	1270	1267	1250	1260
ν V=O	–	–	1079	1093
ν CC	1045	1061	1047	1062
γ HCCC	1009	982	1005	1020
γ HCCN		980	965	974
β OCO	806	805	826	819
γ CCrCN	693	684	–	–
β CNCr	443	392	–	–
β OVO	–	–	450	474
ν VN	–	–		391

ν : Stretching; β : in plane bending; γ : out-of plane bending.

Table 4. Experimental and theoretical electronic transitions, oscillator strength for the complexes **1** and **2**.

Solvent	Exp. λ (nm)	TD-HSEH1PBE/6-311G(d,p)			Major contributions via SWizard//Chemission program
		λ (nm)	Osc. strength	μ_{eg} (D)	
Complex 1					
Ethanol		523	0.0045	0.7090	H→L+1 α (+59%)//Cr(61%)+3-Mepy(27%)+COO ⁻ (12%)→3-Mepy(83%)+COO ⁻ (17%)
					H→L+7 α (+32%)//Cr(61%)+3-Mepy(27%)+COO ⁻ (12%)→Cr(49%)+3-Mepy(26%)+COO ⁻ (25%)
	321	395	0.0402	1.8394	H→L+3 α (+48%)//Cr(61%)+3-Mepy(27%)+COO ⁻ (12%)→Cr(11%)+3-Mepy(77%)+COO ⁻ (12%)
					H→L+1 α (+31%)//Cr(61%)+3-Mepy(27%)+COO ⁻ (12%)→3-Mepy(83%)+COO ⁻ (17%)
	270	269	0.0079	0.6706	H-2→L+3 α (+19%)//3-Mepy(35%)+COO ⁻ (63%)→3-Mepy(77%)+COO ⁻ (12%)
					H-8→L β (+14%)//3-Mepy(30%)+COO ⁻ (68%)→3-Mepy(48%)+COO ⁻ (22%)
	260	259	0.0132	0.8514	H-1→L+5 α (+67%)//3-Mepy(20%)+COO ⁻ (31%)→3-Mepy(96%)+COO ⁻ (4%)
	218	246	0.0287	1.2266	H-2→L β (+12%)//3-Mepy(35%)+COO ⁻ (64%)→3-Mepy(48%)+COO ⁻ (22%)
					H-4→L+1 α (+10%)//3-Mepy(89%)+COO ⁻ (11%)→3-Mepy(83%)+COO ⁻ (17%)
Gas phase		523	0.0085	0.9702	H→L β (+40%)//Cr(56%)+3-Mepy(34%)+COO ⁻ (10%)→Cr(22%)+3-Mepy(60%)+COO ⁻ (18%)
					H→L+3 β (+39%)//Cr(56%)+3-Mepy(34%)+COO ⁻ (10%)→Cr(20%)+3-Mepy(72%)+COO ⁻ (8%)
		414	0.0549	2.1984	H→L+1 α (+46%)//Cr(59%)+3-Mepy(29%)+COO ⁻ (12%)→Cr(1%) +3-Mepy(87%)+COO ⁻ (12%)
					H→L+3 α (+15%)//Cr(59%)+3-Mepy(29%)+COO ⁻ (12%)→Cr(13%)+3-Mepy(78%)+COO ⁻ (9%)
					H→L+4 β (+15%)// Cr(56%)+3-Mepy(34%)+COO ⁻ (10%)→Cr(17%)+3-Mepy(74%)+COO ⁻ (9%)
		270	0.0004	0.1482	H-2→L+1 α (+65%)//3-Mepy(66%)+COO ⁻ (32%)→3-Mepy(87%)+COO ⁻ (12%)
					H-1→L+2 β (+14%)//3-Mepy(33%)+COO ⁻ (66%)→3-Mepy(75%)+COO ⁻ (15%)
	260	0.0165	0.9558	H-9→L β (+18%)//3-Mepy(27%)+COO ⁻ (67%)→3-Mepy(60%)+COO ⁻ (19%)	
				H-2→L+3 α (+17%)//3-Mepy(66%)+COO ⁻ (32%)→3-Mepy(78%)+COO ⁻ (10%)	
	256	0.0022	0.3466	H-3→L+1 β (+26%)//3-Mepy(66%)+COO ⁻ (33%)→3-Mepy(87%)+COO ⁻ (11%)	
				H-6→L β (+20%)//3-Mepy(84%)+COO ⁻ (16%)→3-Mepy(60%)+COO ⁻ (19%)	
				H-8→L β (+15%)//3-Mepy(23%)+COO ⁻ (75%)→3-Mepy(60%)+COO ⁻ (19%)	
Complex 2					
Ethanol		587	0.0002	0.1482	H→L+4 α (+44%)//VO(59%)+3-Mepy(23%)+COO ⁻ (18%)→VO(50%)+3-Mepy(48%)+COO ⁻ (2%)
					H→L+1 α (+25%)//VO(59%)+3-Mepy(23%)+COO ⁻ (18%)→VO(10%)+3-Mepy(80%)+COO ⁻ (10%)
	371	400	0.0007	0.2477	H→L α (+77%)//VO(59%)+3-Mepy(23%)+COO ⁻ (18%)→VO(7%)+3-Mepy(80%)+COO ⁻ (13%)
		271	0.0023	0.3612	H→L+2 α (+60%)//VO(59%)+3-Mepy(23%)+COO ⁻ (18%)→VO(14%)+3-Mepy(77%)+COO ⁻ (9%)
					H→L+4 α (+31%)//VO(59%)+3-Mepy(23%)+COO ⁻ (18%)→VO(50%)+3-Mepy(48%)+COO ⁻ (2%)
		273	0.1835	3.1347	H-2→L β (+39%)//3-Mepy(93%)+COO ⁻ (7%)→3-Mepy(81%)+COO ⁻ (14%)
				H-3→L α (+35%)//3-Mepy(93%)+COO ⁻ (7%)→3-Mepy(80%)+COO ⁻ (13%)	
	210	0.0016	0.2714	H-8→L+1 α (+38%)//3-Mepy(25%)+COO ⁻ (65%)→3-Mepy(80%)+COO ⁻ (10%)	
				H-6→L+1 β (+20%)//3-Mepy(26%)+COO ⁻ (65%)→3-Mepy(83%)+COO ⁻ (11%)	
Gas phase		569	0.0001	0.1296	H→L+4 α (+60%)//VO(59%)+3-Mepy(23%)+COO ⁻ (18%)→VO(67%)+3-Mepy(32%)+COO ⁻ (1%)
					H→L+1 α (+23%)//VO(59%)+3-Mepy(23%)+COO ⁻ (18%)→VO(6%)+3-Mepy(86%)+COO ⁻ (8%)
		429	0.0004	0.1902	H→L α (+78%)//VO(59%)+3-Mepy(23%)+COO ⁻ (18%)→VO(6%)+3-Mepy(84%)+COO ⁻ (10%)
		272	0.0052	0.5475	H-2→L+1 α (+44%)//VO(7%)+3-Mepy(28%)+COO ⁻ (65%)→VO(6%)+3-Mepy(86%)+COO ⁻ (8%)
					H-1→L α (+17%)//VO(1%)+3-Mepy(33%)+COO ⁻ (66%)→VO(6%)+3-Mepy(84%)+COO ⁻ (10%)
		247	0.0923	2.2024	H-3→L α (+27%)//VO(9%)+3-Mepy(50%)+COO ⁻ (41%)→VO(6%)+3-Mepy(84%)+COO ⁻ (10%)
				H-3→L β (+23%)//VO(2%)+3-Mepy(84%)+COO ⁻ (14%)→VO(4%)+3-Mepy(85%)+COO ⁻ (11%)	
	232	0.0064	0.5609	H-2→L+2 α (+53%)//VO(7%)+3-Mepy(28%)+COO ⁻ (65%)→VO(4%)+3-Mepy(90%)+COO ⁻ (6%)	
				H-1→L+3 α (+37%)//VO(1%)+3-Mepy(33%)+COO ⁻ (66%)→VO(1%)+3-Mepy(95%)+COO ⁻ (4%)	

Table 5. The ground and excited dipole dipol moment (μ_g and μ_e , in Debye), the mean linear polarizability ($\langle\alpha\rangle$, in 10^{-24} esu), refractive index (n), linear susceptibility ($\chi^{(1)}$, in 10^{-2} esu), anisotropy of linear polarizability ($\Delta\alpha$, in 10^{-24} esu), mean first- and second-order hyperpolarizabilities ($\langle\beta\rangle$ and $\langle\gamma\rangle$ in 10^{-30} and 10^{-36} esu), first-order static hyperpolarizability (β_0 (two-level model) in 10^{-30} esu), and third-order susceptibility ($\chi^{(3)}$, in 10^{-13} esu) for the complexes **1** and **2**.

Property	HSEh1PBE/6-311G(d,p)			
	Ethanol	Gas phase	Ethanol	Gas phase
	Complex 1		Complex 2	
μ_g	10.7	6.6	2.5	1.7
μ_e	12.4	7.2	1.8	1.2
μ_g (pNA) ^a			6.2 ^a	
μ_g (Urea) ^b			4.56 ^b	
$\langle\alpha\rangle$	60.2	45.2	38.8	29.5
$\langle\alpha\rangle$ (pNA) ^a			17 ^a	
$n_{theo.}$	1.92	1.45	2.40	1.40
n_{exp}		1.39		1.26
$\chi^{(1)}$	25.80	20.58	38.97	14.75
$\Delta\alpha$	6.5	9.7	22.3	19.2
$\langle\beta\rangle$	55.3	30.9	5.0	1.7
β_0	0.341	0.189	-0.166	-0.0255
$\langle\beta\rangle$ (pNA) ^a			9.2 ^a	
$\langle\beta\rangle$ (Urea) ^{b,c}			0.32 ^b , 0.13 ^c	
$\langle\gamma\rangle$	251.0	110.2	37.7	17.2
$\chi^{(3)}$	119.47	25.80	94.26	3.89
$\langle\gamma\rangle$ (pNA) ^a			15 ^a	
$\langle\gamma\rangle$ (Urea) ^c			7 ^b	

^aFrom ref. [85].

^bFrom ref. [87].

^cFrom ref. [88].

Table 6. Protein–ligand interactions, their energy values and in vitro inhibition IC₅₀ values (μM) of the complexes **1** and **2** for α–glucosidase

Compound	IC ₅₀ (μM) ^a	Complex 1- protein interaction	Energy ^c (kcal/mol)	Complex 2- protein interaction	Energy ^c (kcal/mol)
3–Methylpicolinic acid (3-mpaH)	not active		Van der Waals interactions		
Complex 1 [Cr(3-mpa) ₃]	>600	S ^f -LYS-156	-7.1	S-TRP-15	-8.5
Complex 2 [VO(3-mpa) ₂]	>600	M ^f -TYR-158	-5.5	S-ASN-259	-7.3
[Cr(NCS)6-mpa) ₂ ·H ₂ O] ^b	>600	S-TYR-158	-14.1	M-ILE-272	-5.9
Genistein	16.575±0.23	M-SER-240	-7.3	M-ALA-292	-7.7
Acarbose ^c	906	S-SER-240	-4.2	M-GLU-296	-4.1
Resveratrol ^d	12.70	S-ASP-242	-7.2	M-LEU-297	-5.6
		S-HIS-280	-4.3	M-SER-298	-6.0
		M-PRO-312	-7.5		
		M-LEU-313	-8.9		
			Hydrogen bonding interactions		
		S-SER-240	-5.2	M-SER-298	-6.5
		S-ASP-242	-8.6	S-SER-298	-5.0
		M-ARG-315	-2.7		
		E _{total}	-107.3	E _{total}	-97.0

^aIC₅₀ values represent the means ± S.E.M. of three parallel measurements (p < 0.05).

^bFrom ref. [17]

^cFrom ref. [88,89]

^dFrom ref. [90,91]

^eThe values of VDW and H–Bond energy are taken as lower than –4.0 and –2.5 kcal/mol, respectively.

^fM and S indicate the main and side chain of the interacting residue, respectively.

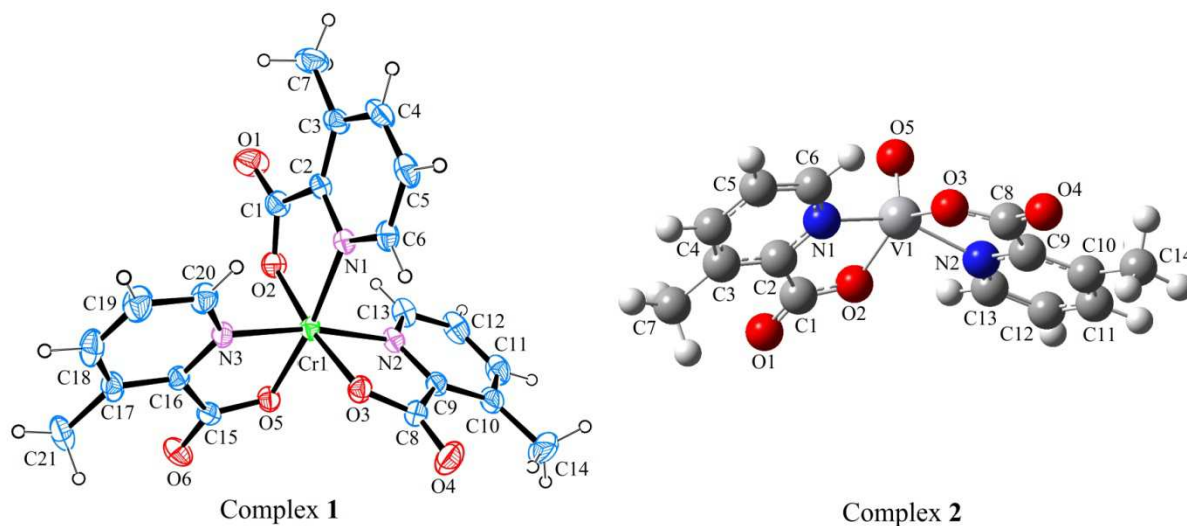


Fig. 1. The single crystal structure of complex **1** and optimized molecular structure of the complex **2** at HSEh1PBE/6-311G(d,p)/LanL2DZ level.

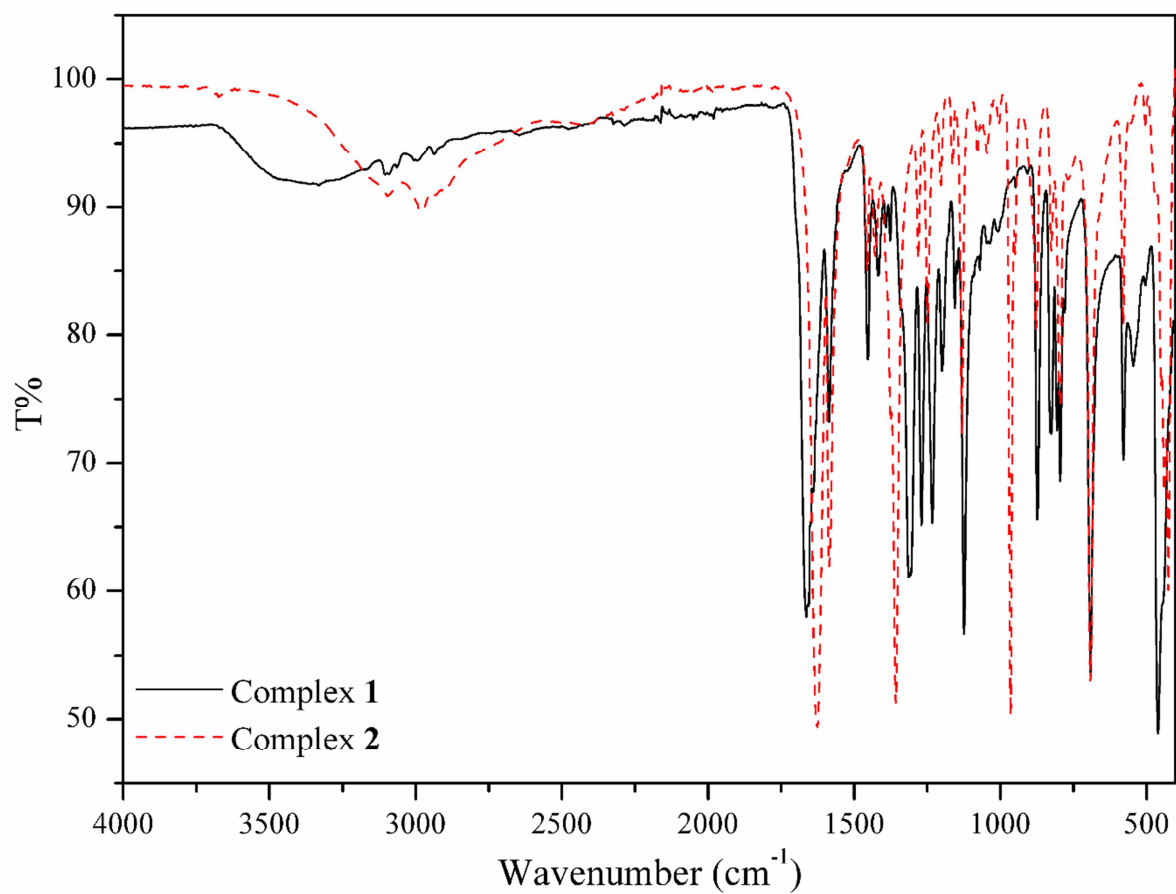


Fig. 2. The FT-IR spectra of the complexes **1** and **2**.

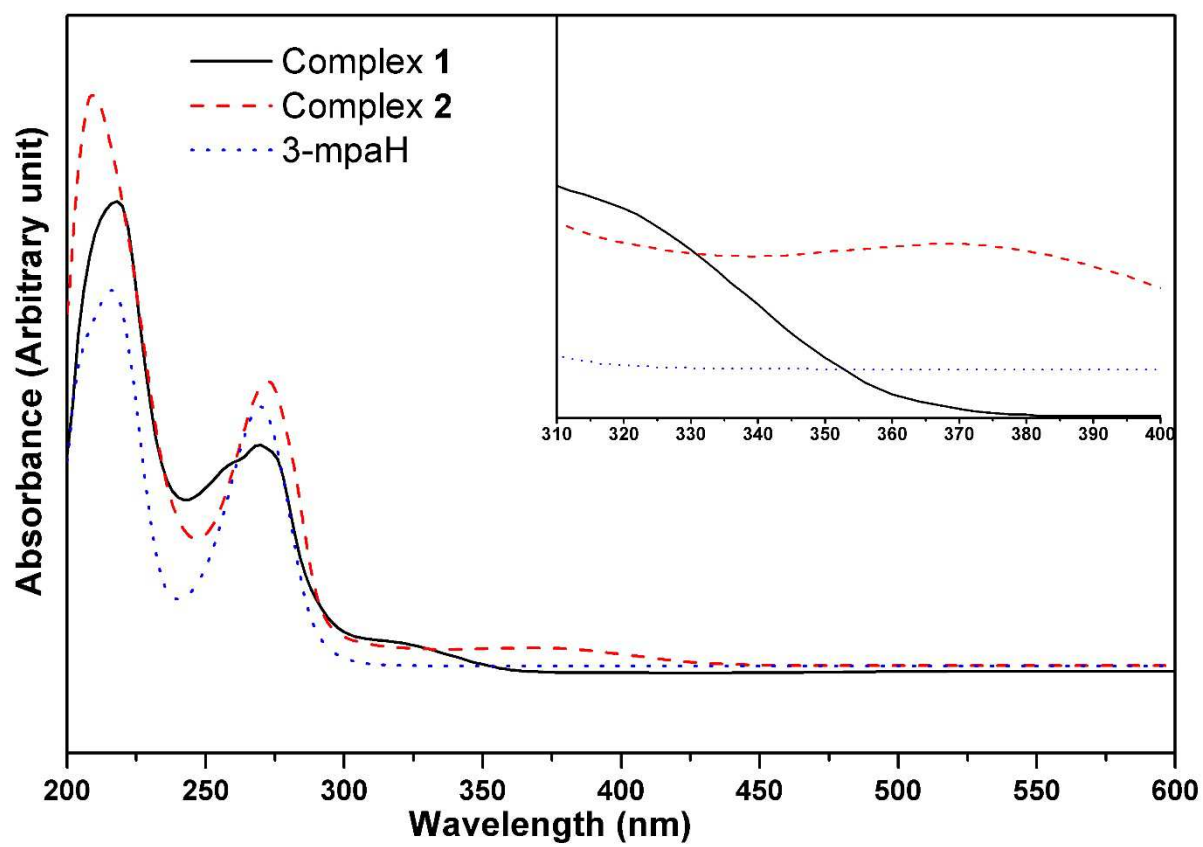


Fig. 3. The UV-vis spectra in ethanol solvent of the 3-mpaH, complexes 1 and 2.

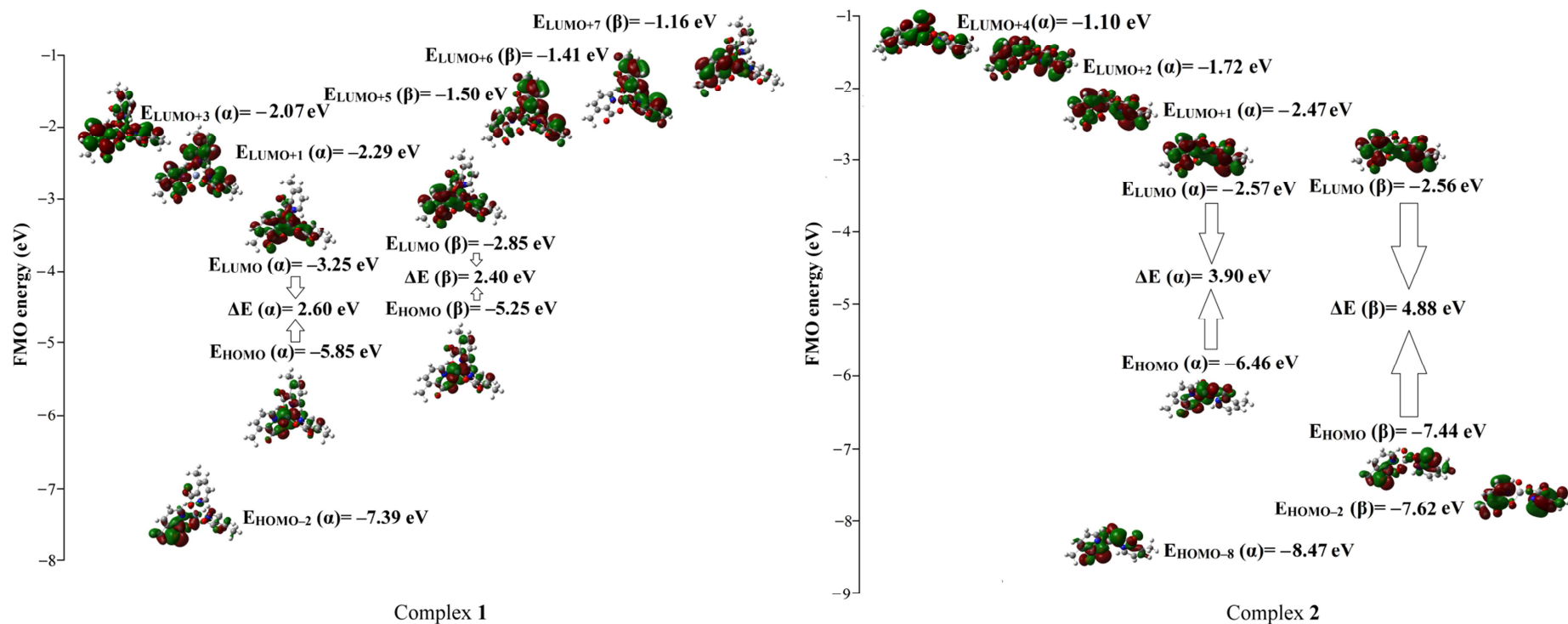


Fig. 4. The most active occupied and unoccupied molecular orbitals in electronic transition of the complexes 1 and 2 obtained by HSEh1PBE level in ethanol solvent.

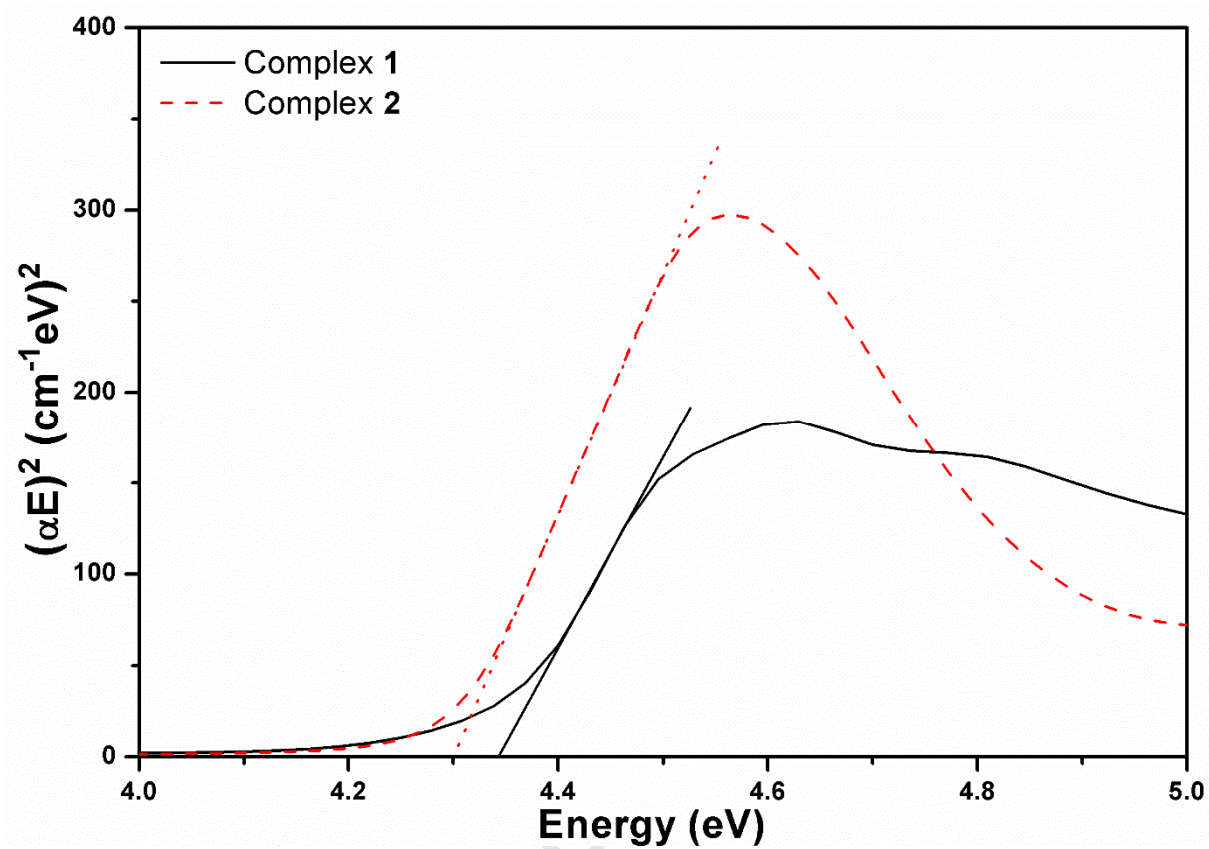


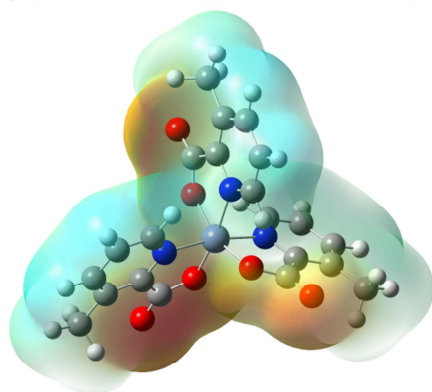
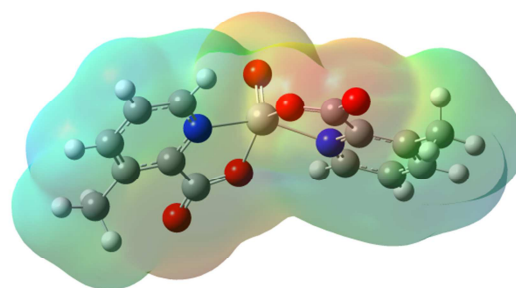


Fig. 5. The graphs of optical band gap energy for the complexes 1 and 2.

$-7.788e-2$  $7.788e-2$ $-6.687e-2$  $6.687e-2$



Complex 1



Complex 2

Fig. 6. Molecular electrostatic potential (MEP) surfaces for the complexes **1** and **2** obtained by HSEh1PBE level in gas phase.

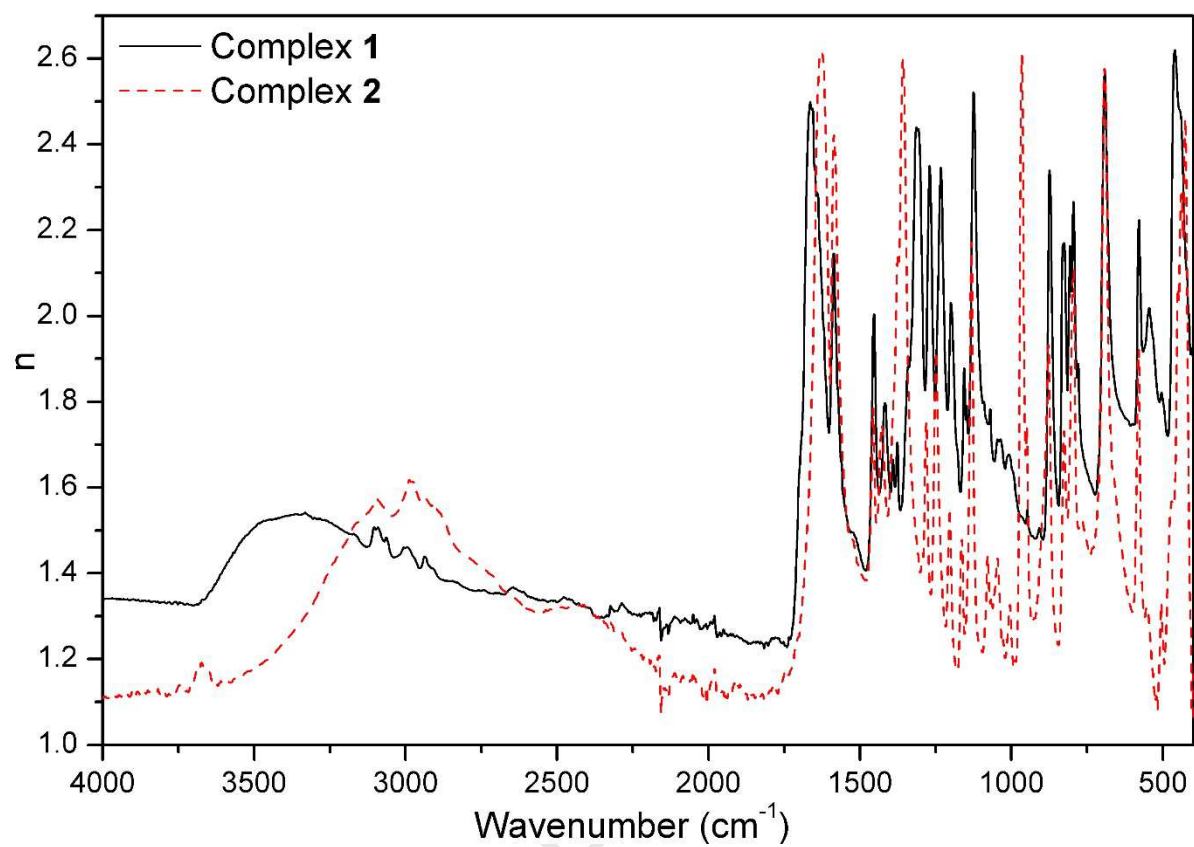
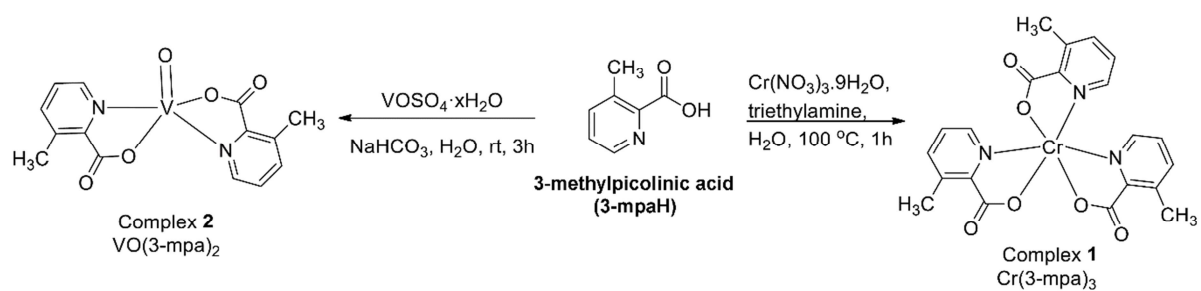


Figure 7. The plot of the refractive index in the IR region for the complexes **1** and **2**.



Scheme 1. The synthesis of the complexes **1** and **2**.

Highlights

- The Cr(III) and V(IV) complexes of 3-methylpicolinic acid (3-mpaH) were synthesized.
- Optical band gap values were obtained by UV–vis spectra.
- The NLO parameters (β , γ and $\chi^{(3)}$) were surveyed.
- The IC₅₀ values of α -glucosidase inhibition for the complexes **1** and **2** were identified.
- TD/DFT calculations were performed to provide deep understanding of the complexes properties.

Declaration of interests

The authors declare that they have no known competing financial interests or personal relationships that could have appeared to influence the work reported in this paper.

The authors declare the following financial interests/personal relationships which may be considered as potential competing interests: